GALEV evolutionary synthesis models
I. Code, input physics and web-interface

Ralf Kotulla[1]⋆, Uta Fritze[1], Peter Weilbacher[2], and Peter Anders[3]: the GALEV team

[1] Centre for Astrophyics Research, University of Hertfordshire, College Lane, Hatfield AL10 9AB, United Kingdom
[2] Astrophysikalisches Institut Potsdam, An der Sternwarte 16, 14482 Postdam, Germany
[3] Sterrekundig Instituut, Princetonplein 5, 3584 CC Utrecht, The Netherlands

arXiv:0903.0378v1 [astro-ph.CO] 2 Mar 2009

ABSTRACT

GALEV evolutionary synthesis models describe the evolution of stellar populations in general, of star clusters as well as of galaxies, both in terms of resolved stellar populations and of integrated light properties over cosmological timescales of $\geqslant 13$ Gyr from the onset of star formation shortly after the Big Bang until today.

For galaxies, GALEV includes a simultaneous treatment of the chemical evolution of the gas and the spectral evolution of the stellar content, allowing for what we call a chemically consistent treatment: We use input physics (stellar evolutionary tracks, stellar yields and model atmospheres) for a large range of metallicities and consistently account for the increasing initial abundances of successive stellar generations.

Here we present the latest version of the GALEV evolutionary synthesis models that are now interactively available at **http://www.galev.org**. We review the currently used input physics, and also give details on how this physics is implemented in practice. We explain how to use the interactive web-interface to generate models for user-defined parameters and also give a range of applications that can be studied using GALEV, ranging from star clusters, undisturbed galaxies of various types E . . . Sd to starburst- and dwarf galaxies, both in the local and the high-redshift universe.

Key words: stars: evolution – galaxies: evolution – galaxies: formation – galaxies: stellar content – galaxies: abundances – galaxies: star clusters

1 INTRODUCTION

GALEV (short for GALaxy EVolution) evolutionary synthesis models have been developed over many years. They were published in several steps and under a variety of first author names, reflecting the number of students who have contributed their respective shares to the development. GALEV models include the spectral evolutionary synthesis of a stellar population with arbitrary star formation history on the basis of the time evolution of the stellar population in the Hertzsprung-Russell diagram, as well as a detailed chemical evolution model for the ISM in terms of a large number of individual element abundances. GALEV models have a wide range of application from star clusters (SCs) to resolved nearby galaxies, to more distant galaxies observed in terms of integrated spectra and photometry, all through galaxies at high redshifts.

Previous applications cover the range from star clusters, normal galaxies E, . . . Sd, dwarf galaxies with and without starbursts, tidal dwarf galaxies, interacting and merging

galaxies with their major starbursts, galaxy transformation processes in galaxy clusters, high redshift galaxies with and without starbursts and post-starbursts and damped Lyman-α absorbers. An early attempt at coupling GALEV evolutionary synthesis models into a cosmodynamical structure formation simulation was presented in Contardo et al. (1998).

GALEV models are now widely used throughout the community. To facilitate access to the latest developments we here present a user-friendly and customized web-interface. It allows access to already available models for the evolution of star clusters of various metallicities, and galaxies of all types both in terms of their time evolution for comparison with observations in the Local Universe and in terms of their redshift evolution. Furthermore it allows the user to run new models for specific applications.

The philosophy for GALEV models is to keep them simple with as small a number of free parameters as possible, and have them predict a large range of observational properties, which – in comparison with observations – constrain the few free parameters. At the present stage, GALEV models are 1-zone models without spatial resolution and without any dynamics included. Future prospects are the consistent inclusion of dust detailing absorption and reemission as a

⋆ E-mail: r.kotulla@herts.ac.uk, u.fritze@herts.ac.uk, pweilbacher@aip.de, p.anders@astro.uu.nl

function of gas content, metallicity and galaxy type, and the coupling with a dynamical model for stars and gas, including a star formation criterion and an appropriate feedback description, to cope with spatially resolved galaxy data.

2   THE GALEV CODE: AN OVERVIEW

2.1   Evolutionary synthesis for star clusters and galaxies

Our GALEV evolutionary synthesis models have many properties in common with the evolutionary synthesis codes from other groups, e.g. BC03 (Bruzual & Charlot 2003), PEGASE (Fioc & Rocca-Volmerange 1997) and Starburst99 (Leitherer et al. 1999), just to name a few, in that all these codes trace the evolution of the stellar population in terms of integrated spectra and/or colours for simple and composite stellar populations.

In contrast to evolutionary synthesis, *stellar population synthesis* (e.g. O'Connell 1976, 1980) or *differential synthesis* (e.g. Pickles 1985a,b; Pickles & Visvanathan 1985) attempts to find the best linear combination of stellar spectra from some library to fit an observed galaxy spectrum . This approach usually achieves very good fits but is limited to a *status quo* description and has difficulties to prove the uniqueness of its solutions. The existence of a stellar Initial Mass Function (IMF) and some continuous Star Formation History (SFH) can be imposed as boundary conditions via Lagrangian multipliers. The major advantages of the population synthesis approach are that it can give valuable first guesses for unknown SFHs and that it allows for unexpected solutions.

All *evolutionary synthesis* models, on the other hand, have to assume a stellar IMF and a SFH, i.e. the time evolution of the SFR for the galaxy. They use stellar evolutionary tracks or isochrones that have to be complete in terms of all relevant stellar evolutionary stages.

Both methods need stellar spectral libraries that also have to be complete in terms of stellar effective temperatures T_{eff}, surface gravities $\log(g)$, and metallicities [Fe/H].

GALEV models are available for a range of stellar IMFs, including Salpeter (1955), Kroupa (2001), and Chabrier (2003). Other choices of the IMF can easily be customized.

For the case of a simple stellar population (SSP), i.e. a star cluster, the SFH is a δ-function, meaning that all stars are formed in a single timestep. GALEV models for SSPs of different metallicities (Kurth et al. 1999; Schulz et al. 2002; Anders & Fritze 2003; Lilly & Fritze 2006) were shown to well reproduce observed colours and spectral indices of star clusters as function of age and metallicity. They also show a pronounced non-linearity at metallicities close to and above the solar value. Important results include the findings that any colour-to-age or index-to-age calibration/transformations are only valid *at one metallicity* and that any colour-to-metallicity or index-to-metallicity calibration/transformations are only valid *at a given age* (cf. Schulz et al. 2002), and that extrapolating observational relations beyond their calibration range lead to significantly misleading results.

In Anders & Fritze (2003) we demonstrated the importance of nebular emission lines and continuum for young stellar populations and showed that they can account for as much as $50 - 60\%$ of the flux in broad-band filters, in particular at low metallicities.

For the description of undisturbed galaxies, SFHs have been determined for normal average galaxies of types E, S0, Sa, Sb, Sc, Sd (cf. Sect. 5.2), that, in combination with a Salpeter IMF extending from a lower mass limit of 0.1 M$_\odot$ (roughly the hydrogen burning limit) to an upper mass limit around $70 - 120$ M$_\odot$, depending on the set of isochrones (cf. Sect. 3.1) selected, provide agreement with average observed galaxy properties in terms of colours, spectra, luminosities, abundances, and gas content. We stress that our galaxy types are meant to denote *spectral types* and we caution that the one-to-one correspondence between spectral and morphological types observed in the Local Universe might not hold to arbitrarily high redshifts.

While in terms of spectral evolution of the integrated light of galaxies (or star clusters) our models are comparable to other evolutionary synthesis models, they go beyond those in that they also allow to describe and analyze resolved stellar populations in terms of colour-magnitude diagrams (CMDs) and in that they self-consistently describe the chemical evolution of the ISM in galaxies together with the spectral evolution of the stellar populations (for the latter see Sect. 2.3), allowing to realistically account for the coexistence of stellar subpopulations of different metallicities observed in local galaxies.

Most of the aforementioned capabilities are not entirely new. Models of the photometric evolution of galaxies date back to Tinsley (1967, 1968, 1972), the first spectroscopic models appeared roughly a decade later (Bruzual A. 1983; Guiderdoni & Rocca-Volmerange 1987). Models of the chemical evolution of galaxies (e.g., Truran & Cameron 1971; Tinsley 1972; Matteucci & Padovani 1993) were capable of taking the increasing enrichment of subsequent stellar populations into account when computing colours (see also, e.g., Matteucci & Tornambe 1987; Fritze et al. 1989), spectra (e.g., Bressan et al. 1994; Fritze & Gerhard 1994a; Fioc & Rocca-Volmerange 1997; Pipino & Matteucci 2004) and line indices (e.g., Weiss et al. 1995; Bressan et al. 1996). Silva et al. (1998) were the first to include a radiative transfer code into their model and could hence extend the wavelength coverage into the (far-)infrared. However, only very few models (e.g., Prantzos et al. 1994; Portinari et al. 1998) exist that take the metallicity dependence of stellar yields into account and hence merit to be called *chemically consistent*. Those, unlike GALEV presented here, mainly focus on the metallicity distribution in the solar neighbourhood and only derive a detailed chemical evolution but no spectral or photometric evolution.

2.2   Chemical evolution of galaxies

Modeling the chemical evolution of galaxies starts from a gas cloud with given initial (e.g. primordial) abundances and given mass. A modified version of Tinsley's equations (Tinsley 1968), including detailed stellar yields, is solved to study the chemical enrichment history of galaxies of different spectral types. This requires knowledge of stellar yields, i.e. production rates of different elements and isotopes, including contributions from SN Ia, as well as stellar lifetimes as function of stellar mass *and metallicity*, that can be taken

from nucleosynthesis and stellar evolution models, respectively.

Closed-box models can be compared to models with specified in- and outflow rates and abundances. We follow the chemical evolution of a large number of chemical elements H, He, ... Fe, fully accounting for the time delay between SF and the return of material in stellar winds, PNe, and SNe.

2.3 Chemically consistent GALEV models for galaxies

Combining the chemical evolution of ISM abundances and the spectral evolution of the stellar population thus allows for what we call a chemically consistent treatment of both the chemical evolution of the ISM and the spectral evolution of the stellar population in galaxies: we use input physics (stellar evolutionary tracks, model atmospheres, stellar lifetimes and yields) for a large range of metallicities and consistently account for the increasing initial abundances of successive stellar generations.

Broad stellar metallicity distributions have been reported for the Milky Way disk (Rocha-Pinto & Maciel 1998), bulge (Sadler et al. 1996; Ramírez et al. 2000), and halo (Ak et al. 2007), as well as for the nearby elliptical galaxy NGC 5128 (Harris et al. 1999; Harris & Harris 2000).

Depending on the SFH of the respective galaxy type and eventually its infall rate, stars of different ages within a galaxy will have different metallicities and obey an age-metallicity relation determined by their galaxy's SFH.

An important consequence of this coexistence of stars with different ages and metallicities is that stars of different metallicities and different ages dominate the light in different wavelength regions. It has severe implications for metallicity indicators defined in different wavelength regimes, which cannot be expected to trace one and the same stellar metallicity. It also affects some widely used SF indicators and modifies, e.g., the calibrations for SFRs from Hα or [OII] fluxes, as well as from FUV luminosities (cf. Bicker & Fritze 2005).

Our GALEV code can model the spectral and chemical evolution of galaxies with arbitrary IMF and SFH over cosmological timescales, from the very onset of SF all through a Hubble time. In combination with a cosmological model we can follow the redshift evolution of galaxies from the early universe until today (Bicker et al. 2004). It also allows to directly study the impact of evolutionary corrections as well as of the chemically consistent treatment as compared to using solar metallicity input physics only (cf. Kotulla & Fritze 2009).

2.4 Colour magnitude diagrams

Despite simplifications the CMDs are valuable tools to study systematic effects of SFH recovery from observations. Fritze & Lilly (2007) and Lilly & Fritze (2008) investigated the accuracy of recovering SFHs from CMDs as a function of the ages of various subpopulations. In addition, they compared their results with the accuracies of recovering SFHs from integrated spectra, multi-band photometry, or Lick indices. These systematic studies are essential for more dis-
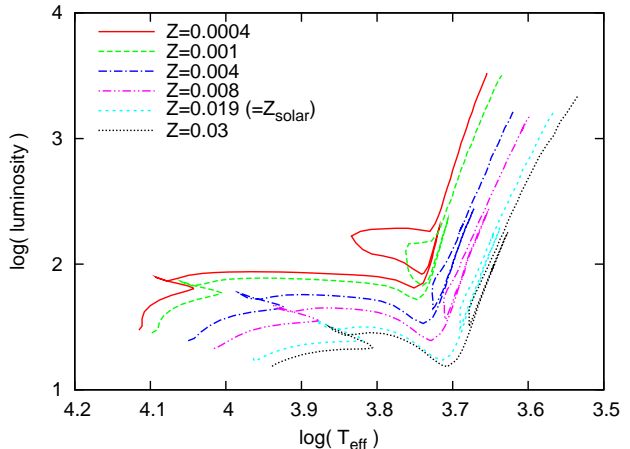

Figure 1. Stelar evolutionary tracks of a $2\,\mathrm{M_\odot}$ star for different metallicities ranging between Z $=$ 0.0004 $=$ $1/50\,\mathrm{Z_\odot}$ and Z $=$ $0.03 = 1.5\,\mathrm{Z_\odot}$.

tant unresolved stellar populations. Moreover, since synthetic CMDs can be calculated in any desired filter combinations, they can be used to optimize observational strategies with respect to the optimal filter combination, e.g. to disentangle ages and metallicities of young, intermediate-age or old stellar populations.

3 INPUT PHYSICS

In the following sections we will review the input physics we use for our GALEV models.

3.1 Stellar evolutionary tracks and/or isochrones

Data for stellar evolution can be taken either from isochrones or stellar evolutionary tracks, both having their advantages and disadvantages. GALEV models currently use the most recent consistent set of theoretical isochrones from the Padova group (Bertelli et al. 1994, ff) for five different metallicities [Fe/H] $= (-1.7; -0.7; -0.4; 0.0; +0.4)$ and include the TP-AGB phase, the importance of which was shown in Schulz et al. (2002). In order to be able to fully account for emission lines we also include the Zero Age Main Sequence (ZAMS) into our models. The isochrone for this ZAMS includes stars up to $120\,\mathrm{M_\odot}$ and is created from the unevolved first data points of the stellar evolutionary tracks. For more details we refer the reader to Bicker & Fritze (2005).

In Fig. 1 we show stellar evolution tracks for a $2\,\mathrm{M_\odot}$ star for 6 different metallicities ranging from Z $= 0.0004 =$ $1/50\,\mathrm{Z_\odot}$ to Z $=$ $0.03 = 1.5\,\mathrm{Z_\odot}$ (Girardi et al. 2000). The general shape remains unchanged with changing metallicity, but low-metallicity tracks are shifted towards increasing luminosities and higher effective Temperatures, i.e. towards the top left in the Hertzsprung-Russell diagram. This behaviour is the same for stars of all masses, in the sense that with decreasing metallicity stars become more luminous and their spectra shift towards higher effective temperatures. It is therefore crucial to include those effects to obtain a consistent picture of galaxy evolution.
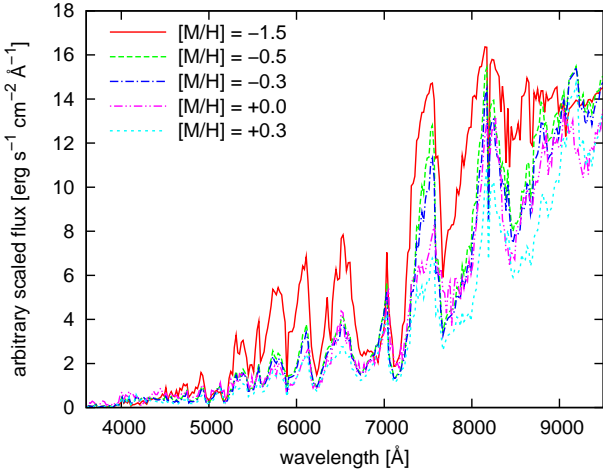
Figure 2. Stellar spectra from the Lejeune library for a star with identical $T_{\rm eff} = 3000$K and $\log g = 4.0$, but different metallicities from $[{\rm M/H}] = -1.5 \ldots + 0.3$.

3.2   Library of stellar spectra

In principle, every library of stellar spectra – observed or theoretical – can be used, provided it is complete in terms of stellar $T_{\rm eff}$, $\log(g)$, and [Fe/H]. GALEV assigns spectra to stars in the isochrones according to each star's metallicity, effective temperature $T_{\rm eff}$ and surfce gravity $\log(g)$, normalising the spectra with the star's luminosity (for details see Sect. 4.1). So far, GALEV uses the BaSeL library of model atmospheres from Lejeune et al. (1997, 1998), originally based on the Kurucz (1992) library. The wavelength coverage spans the range from the XUV at $\lambda \approx 90$ Å to the FIR at $\lambda = 160\,\mu$m, with a spectral resolution of 20 Å in the UV-optical and $50-100$ Å in the NIR range. We remind the reader that there are significant contributors other than starlight (e.g. PAHs, thermal emission from cold dust) at wavelengths beyond the K-band, that are not currently included in our models. This wavelength range should hence be used with caution.

Stellar spectra are heavily influenced by metallicity due to the increased absorption line strength (e.g. for Fe-lines) and line-blanketing with increasing abundances. In Fig. 2 we show the example of a cool star ($T_{\rm eff} = 3000$K, $\log g = 4.0$) from the above mentioned BaSeL library. The effects of metallicity are stronger for cool stellar atmospheres where molecular absorption by VO, TiO, NH_4, H_2O etc. plays a larger role (Allard et al. 2000; Kučinskas et al. 2006).

3.3   Gaseous emission: lines and continuum

In addition to the stellar absorption spectra we also compute line and continuum emission from gas ionized by hot massive stars.

We do not take the ionizing photons from the stellar spectral library, but instead use the tabulated values from Schaerer & de Koter (1997) for $N_{\rm LyC}$ as a function of stellar effective temperature, radius, and metallicity. They yield much better agreement with observations as well as with recent results from expanding non-LTE, line-blanketed models atmosphere calculations by Smith et al. (2002).

We can then compute the total flux emitted by the gas per unit wavelength as

$$F_\lambda = \frac{\gamma_\lambda(T)}{\alpha^{(2)}(T)} N_{LyC} = \frac{c}{\lambda^2} \frac{\gamma_\nu(T)}{\alpha^{(2)}(T)} N_{LyC} \qquad (1)$$

with the speed of light c, electron temperature $T = 10\,000$ K, and total recombination coefficient $\alpha^{(2)}(10\,000\,{\rm K}) = 2.575 \times 10^{-13}\,{\rm cm}^3\,{\rm s}^{-1}$ (Aller 1984). The gas continuum coefficients are then computed for $T = 10\,000$ K following Ercolano & Storey (2006) that contains an algorithm to compute the bound-free radiation for hydrogen and helium ($\gamma_{\rm HI}$, $\gamma_{\rm HeI}$, and $\gamma_{\rm HeII}$). The HI two-photon emission coefficient $\gamma_{\rm H2p}$ is taken from Nussbaumer & Schmutz (1984) and for the free-free emission $\gamma_{\rm b}$ we use the formula from Brown & Mathews (1970) and compute the Gaunt factors using the algorithm from Hummer (1988). All γ-factors are summed to form the final:

$$\gamma_\nu = \gamma_{\rm b} + \gamma_{\rm H2p} + \gamma_{\rm HI} + \frac{n_{\rm He^+}}{n_{\rm H^+}}\gamma_{\rm HeI} + \frac{n_{\rm He^{++}}}{n_{\rm H^+}}\gamma_{\rm HeII}. \qquad (2)$$

For the densities of the helium He I and He II ions relative to H I we use values typical for H II regions in galaxies (Ercolano, priv. comm.), 0.0897 and 1.667×10^{-4} for He I and He II, respectively. The final isochrone spectra are not very sensitive to slight changes in these values.

The line strengths of the hydrogen lines are computed using atomic physics and the emission rate of ionizing photons $N_{\rm LyC}$ from O- and early B-stars. From the number of ionizing photons, $N_{\rm LyC}$, we compute the flux in the Hβ line using

$$f(H\beta) = 4.757 \times 10^{-13}{\rm erg} \times N_{\rm LyC}. \qquad (3)$$

Assuming Case B recombination for a pure hydrogen cloud with $T_{\rm e} = 10\,000$ K (Osterbrock & Ferland 2006), we can then derive the line strengths of all other hydrogen lines. Line strengths for heavier elements are computed using metallicity-dependent line-ratios relative to Hβ. For metallicities $[{\rm Fe/H}] \geqslant -0.4$ those are taken from the Stasińska (1984) photoionization models, adopting typical Galactic values of $T_{\rm e} = 8100$ K and $n_{\rm e} = 1$ cm^{-3} for electron temperature and density. For lower metallicities, we use observed line ratios from Izotov et al. (1994, 1997) and Izotov & Thuan (1998). These are supposed to include systematic changes in $T_{\rm e}$, $n_{\rm e}$ and the ionizing radiation field in lower metallicities environments (cf. Anders & Fritze 2003). Note that we do not include detailed radiation transfer calculations (as, e.g., in Garcia Vargas & Diaz 1994; Ferland et al. 1998; Ercolano et al. 2003), hence we caution the user to use line-ratios for detailed line diagnostics. We correct the gaseous emission for small amounts of dust within the HII regions by reducing the ionizing flux by 30% if the gaseous metallicity is near solar, i.e. for $[{\rm Fe/H}] \geqslant -0.4$. For lower metallicities we use the full ionizing flux since those environments are essentially dust-free (Mezger 1978). We do not account for yet unknown amounts of dust depletion of heavy elements within the HII regions. However, in the case of low-metallicity galaxies these effects are already included in the observed line-ratios.

Note that we do not account for internal self-absorption of Lyman continuum photons within the HII regions or the surrounding galaxy, since the fraction of flux leaking out of these regions is still a matter of ongoing debate (see, e.g., Ferguson et al. 1996; Castellanos et al. 2002;
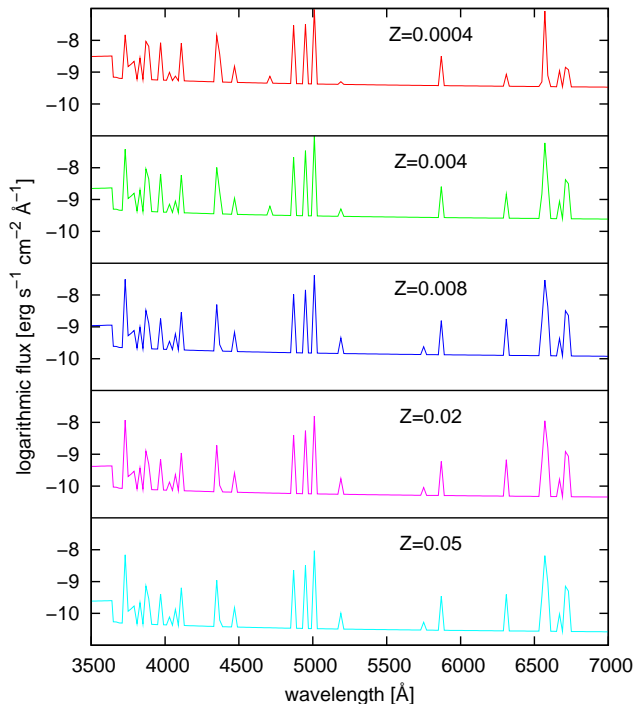
3.4 Lick stellar absorption indices

Since the resolution of the Lejeune et al. (1997, 1998) library is not sufficient to calculate Lick absorption indices directly from the spectra, GALEV models use the empirical calibrations presented by Gorgas et al. (1993), Worthey et al. (1994) and Worthey & Ottaviani (1997). From those, GALEV calculates the fluxes in the Lick indices for every star, sums them up for the entire stellar population at every timestep to yield integrated index fluxes and, in combination with continuum fluxes from the integrated absorption line spectra, the respective index equivalent widths (Kurth et al. 1999; Lilly & Fritze 2006). GALEV at the present stage includes the following Lick indices: $H\delta_A$, $H\gamma_A$, $H\delta_F$, $H\gamma_F$, CN_1, CN_2, Ca4227, G4300, Fe4383, Ca4455, Fe4531, Fe4668, $H\beta$, Fe5015, Mg_1, Mg_2, Mgb, Fe5270, Fe5335, Fe4506, Fe5709, Fe5782, NaD, TiO_1, and TiO_2 (see Trager et al. 1998, and references therein for all index definitions).

3.5 Stellar yields

To model the chemical enrichment histories of galaxies, GALEV uses stellar yields for a large number of individual elements (H, He, Li, Be, B, C, N, O, F, Ne, Na, Mg, Al, Si, P, S, Cl, Ar, K, Ca, Sc, Ti,V, Cr, Mn, Fe, Co, Ni, Cu, Zn, Ga, Ge) from Woosley & Weaver (1995) for massive stars and from van den Hoek & Groenewegen (1997) for low-mass stars of various metallicities. Stellar lifetimes are taken from the isochrones. There is a minor inconsistency in doing so, since Woosley & Weaver (1995) used models without mass-loss, while current isochrones in general account for mass-loss. However, since yields are only available for a very coarse metallicity grid this does not significantly affect the resulting chemical evolution. GALEV also includes type Ia SN yields for the carbon deflagration white dwarf binary scenario (W7) from Nomoto et al. (1997). See Lindner et al. (1999) for a detailed description of the chemically consistent chemical evolution aspects of GALEV.

3.6 Ejection rates and remnant masses

One of the central input parameters for GALEV is the time-dependent ejection rates necessary to compute the chemical evolution of galaxies. Those rates are derived from the initial stellar masses $M_\star$ and the remaining remnant masses m_R. For stars with masses $M_\star \geqslant 30\,M_\odot$ the remnant is assumed to be a black hole of $m_{BH} = 8.0\,M_\odot$, with the remaining mass being returned to the ISM; stars with initial masses of $30\,M_\odot \geqslant M_\star \geqslant 6.0\,M_\odot$ result in a neutron star of mass m_{NS} given by Nomoto & Hashimoto (1988):

$$m_{NS}[M_\odot] = 1.02 + 3.6363 \times 10^{-2}(M_\star/M_\odot - 8.0)M_\odot;$$

For the mass range of $6.0\,M_\odot \geqslant m_\star \geqslant 0.5\,M_\odot$, for which the stellar remnant is a white dwarf, we use a fit to the data points of Weidemann (2000):

$$m_{WD}[M_\odot] = 0.444 + 0.0838(M_\star/M_\odot);$$

This, combined with the extrapolation of the NS relation down to $6\,M_\odot$, provides a better matched connection between the two mass ranges. while being compatible with the slightly steeper slope derived by Kalirai et al. (2008). However, as the remnant is only used to derive the mass returned
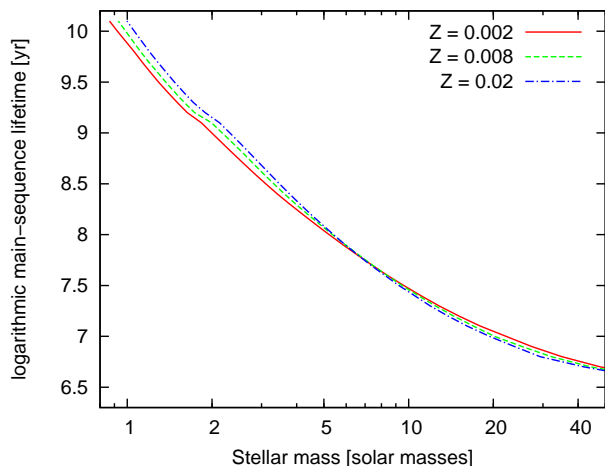

Figure 3. Emission line spectrum of the 4 Myr isochrone for 5 different metallicities ranging between Z = 0.0004 ([Fe/H] = −1.7) and Z = 0.05 ([Fe/H] = +0.4).

Fernández-Soto et al. 2003; Inoue et al. 2005; Siana et al. 2007; Wise & Cen 2008).

Depending on application, our models can include both continuum and line emission, continuum emission only or no gas emission at all. In Krüger et al. (1995) and Anders & Fritze (2003) we showed that in the case of Blue Compact Dwarf galaxies and in young and metal-poor SSPs, gaseous emission can contribute as much as 60% to the flux in broad-band filters. Emission lines are the dominant contributors in the optical, whereas continuum emission dominates in the NIR.

Combining the effects of higher luminosities and higher effective temperatures with the effects of longer lifetimes of high-mass stars at low metallicities has a profound impact on the spectrum of galaxies. All three factors lead to bluer colours, higher overall luminosities and as a further aspect significantly stronger gaseous emission, i.e. gaseous continuum and line emission.

In Fig 3 we show the gaseous emission spectra for isochrone spectra at an age of 4 Myr and for 5 metallicities from $1/50\,Z_\odot$ to $2.5\,Z_\odot$. The first notable aspect is the overall emission line strength that is higher by a factor of about 10 comparing the two extreme cases. But also the individual line ratios change significantly, i.e. the ratio between $H\alpha$ (6563 Å) and [N II] (6583 Å) ($H\alpha$/[NII] $\approx$ 48 at low metallicity and $\approx$ 7 for solar metallicities). This extreme ratio is directly affected by the lower nitrogen abundance at low metallicity. Other line ratios, e.g. [O II] (3727 Å) to [O III] (5007 Å) also change due to the more intense radiation field coming with the low metallicity environment.

Figure 4. Main-sequence lifetimes as function of initial stellar mass for three different metallicities.

to the ISM during its lifetime and death, the exact transition point from neutron star to white dwarf is of minor importance.

Stars with masses $m_\star \lesssim 0.5 M_\odot$ have lifetimes in excess of a Hubble time and negligible winds, hence do not return any material to the ISM.

In Fig. 4 we show the main-sequence lifetimes of stars as function of initial mass for three different metallicities from $Z = 0.002 = 1/10\, Z_\odot$ to $Z = 0.02 = Z_\odot$, based on data from Marigo et al. (2008) for $M_\star < 7\, M_\odot$ and Bertelli et al. (1994) for $M_\star > 7 M_\odot$. Low-mass stars live longer at high metallicities, while high-mass stars have longer lifetimes for lower metallicities; stars with masses $\approx 3 - 4 M_\odot$ have roughly the same lifetimes independent of metallicity (see Fig. 4). The $20 M_\odot$ star for example has a 10% increased lifetime at $Z = 1/10\, Z_\odot$ as compared to $Z = Z_\odot$.

3.7 Filter functions and magnitude systems

GALEV includes a large number of filter functions to be convolved with the model spectra in order to avoid uncertainties associated with transformations between filter systems. It also provides the option to choose the desired magnitude system Vegamag, ABmag, and STmag to be directly comparable to observations and avoid transformations between different magnitude systems. Magnitudes in the Vegamag systems are defined to have magnitude zero for an A0V star; we use the Vega-spectrum from the Lejeune et al. (1997, 1998) library combined with the flux calibration from Bohlin & Gilliland (2004) as our standard star. AB magnitudes (Oke 1974; Bohlin & Gilliland 2004) are derived from the monochromatic flux f_ν such that $m_{AB} = -2.5 \log(f_\nu) + 48.6$ if f_ν is measured in $\mathrm{erg\, s^{-1}\, cm^{-2}\, Hz^{-1}}$; a colour of 0 in the AB magnitude means that the object emits constant flux per unit *frequency* interval; analogous to the above, colours of 0 in the ST magnitude systems mean constant emitted flux per unit *wavelength* interval. The zeropoint has been chosen such that a source with $f_\lambda = 3.63 \times 10^{-9} \mathrm{erg\, s^{-1}\, cm^{-1}\, \mathring{A}^{-1}}$ has $m_{ST} = 0\,\mathrm{mag}$ in all filters.

Our current database contains filters from all major telescopes and instruments, including all HST instruments (incl. WFC3), many ESO instruments, and all common filter sets like Johnson/Cousins, Strömgren, Washington, and SDSS. However, note that due to the wide wavelength sampling of 20 Å of the current spectral library, narrow-band filters cannot be adequately supported at this stage.

3.8 Dust extinction

To account for extinction and reddening due to interstellar dust, GALEV also implements the most commonly used empirical extinction laws from Calzetti et al. (2000) and Cardelli et al. (1989). The earlier was derived from actively star-forming galaxies and describes a relatively gray extinction without the 2175 Å bump, characteristic for the latter extinction law. For the Cardelli law we assume a mean extinction parameter of $R_V = A(V)/E(B - V) = 3.1$, characteristic for relatively quiescent galaxies. Although models exists that offer a more detailed treatment of dust extinction and in some cases dust emission (see, e.g., Silva et al. 1998; Popescu et al. 2000; Cunow 2001, 2004; Dopita et al. 2005; Möllenhoff et al. 2006; Piovan et al. 2006a,b), the major drawback of these models is that they in general require assumptions on the geometry and spatial distribution of dust, gas and stars. However, the aim of GALEV is to describe the spectrum of the average represantation of each galaxy type, making if difficult to compare these two approaches.

3.9 Cosmological model

GALEV can also be coupled to a cosmological model to describe the evolution of galaxies as function of redshift. For this purpose we have to convert ages into redshifts and vice versa. In its current version we implemented a flat cosmology ($\Omega_K = 0$). The choice of the local Hubble constant H_0, the density parameters Ω_M and Ω_Λ (with the additional constraint $\Omega_M + \Omega_\Lambda = 1$) and the galaxy formation redshift z_{form} then completely determine the galaxy age as function of redshift. Because of the short time interval between e.g. $z = 12$ and $z = 5$, the exact value of z_{form} has very little impact, hence we choose an intermediate value of $z_{form} = 8$ as our default.

3.10 Intergalactic attenuation

To correctly describe spectra of higher redshift galaxies one has to include the absorption shortwards of the Lyman-α line due to intervening neutral hydrogen clouds. For that reason GALEV implements the description for the average attenuation effect as function of redshift following Madau (1995) and covering the range $0 \leqslant z \leqslant 7$.

4 PROGRAM STRUCTURE

The actual modeling process with GALEV can be divided into three steps:

(i) In the first step GALEV convolves the isochrones of each age-metallicity combination with the specified IMF, normalized to $1\, M_\odot$. It then assigns a spectrum from the

stellar library to each star on each isochrone and computes the integrated isochrone spectrum. Then the gaseous continuum emission and emission lines are added to the young isochrone spectra. Using the yield tables and stellar remnant masses described in Sect. 3.5 with stellar lifetimes from the isochrones, GALEV also derives the gas and metal ejection rates needed for the chemical evolution.

(ii) In the second step GALEV computes the chemical and spectral evolution of the desired stellar population. For each timestep the current isochrone spectra are weighted with the SFH. The contributions from older SF episodes are obtained by integration over all past timesteps. The required interpolations in age and metallicity are described below. GALEV thus calculates the time evolution of the integrated spectrum and its resulting line strength (i.e. Lick-) indices of a simple (SSP, star cluster) or composite (galaxy) stellar population, including the gaseous emission where appropriate. From the ejection rates and the available gas mass GALEV calculates the new gaseous metallicity that will be used for stars born during the next timestep.

(iii) In the last step GALEV converts the integrated spectra into magnitudes in a large number of filters. Given a list of requested filters it convolves the spectra with the filter functions and applies zero-points to yield absolute magnitudes for each timestep. It can alternatively be combined with a cosmological model to yield apparent and absolute magnitudes as function of redshift. If requested it also accounts for dust extinction using observed extinction laws and, in the context of cosmological evolution, also for the attenuation by intergalactic neutral hydrogen.

This process is also explained in a more vivid step-by-step explanation in appendix A.

4.1 Computation of isochrone spectra

A crucial step is the assignment of stellar spectra from the library to the points describing the isochrones. Since the available stellar parameters $T_{\rm eff}$ and $\log(g)$ in the library often do not match those required by the isochrones, GALEV has to interpolate between them in both $T_{\rm eff}$ and $\log(g)$. For a given combination of $T_{\rm eff}$ and $\log(g)$ this is done as follows:

(i) Find up to four spectra bracketing the required values in both $T_{\rm eff}$ and $\log(g)$.

(ii) Interpolate the spectra to the required value of $T_{\rm eff}$ in each pair of lower (upper) values of $\log(g)$, yielding two new interpolated spectra with the correct $T_{\rm eff}$ and different $\log(g)$. An important factor during this interpolation is the weighting of the spectra with each star's luminosity given by the isochrone. We choose to use the integrated luminosity in the Johnson-V or Bessell-H-band, depending on the temperature of the star given by $T_{\rm eff}$. The original approach to normalize all stars in the V-band turned out to be insufficient for cool giants with only little flux in the optical. A "cool giant" in this context is defined by $T_{\rm eff} \leqslant 3500$ K and $\log(g) \leqslant 3.5$.

(iii) The spectrum for the required value of $\log(g)$ is then obtained by interpolation between the two spectra with the right $T_{\rm eff}$, again weighting with each star's respective luminosity.

For the very hot stars ($T_{\rm eff} > 50\,000$ K), the BaSeL stellar library does not provide spectra. In those cases we extend the spectral library by approximating the missing stellar spectra with black-body spectra of the requested temperatures. The validity of this approximation for wavelengths longwards of $\lambda \approx 230$ Å is supported by only minor differences between pure black-body and true spectra from both observations (Gauba et al. 2001) and modelling (Rauch 2003) of very hot central stars of planetary nebulae.

In a final step, all isochrone spectra are normalized to a distance of 10 pc, and are given in units of erg s^{-1} cm^{-2} Å^{-1}.

4.2 Interpolation of isochrone-spectra and integration of galaxy spectra

One important aspect of GALEV is how to interpolate between the isochrone spectra of different ages and metallicities, in other words how to map the coarse grid of isochrones available onto the finer grid needed for galaxies. GALEV here interpolates logarithmically between ages and linearly between metallicities expressed as $\log(Z) \sim {\rm [Fe/H]}$. During their very early stages the gaseous metallicities of galaxies are lower than the metallicity of the lowest metallicity isochrone with ${\rm [Fe/H]} = -1.7$. For stars born at these stages, we chose to use the lowest metallicity isochrone to avoid the uncertainties in an extrapolation to lower metallicities. The same is done for stars born from gas with a metallicity higher than the highest metallicity isochrone. For these stars we use the highest metallicity isochrone available with ${\rm [Fe/H]} = +0.4$.

5 CALIBRATION OF THE GALEV MODELS AND COMPARISON TO OBSERVATIONS

We stress that with the input physics as outlined above, a stellar IMF with lower and upper mass limits chosen and total mass of the galaxy or star cluster specified, GALEV models provide the time evolution of spectra, luminosities, and colours *in absolute terms*. The same holds true for the gas content and the chemical enrichment of galaxies. *No a posteriori* gauging is applied.

The only exception is the cosmological context for galaxies: before luminosities and magnitudes of redshifted galaxies are calculated, the B-band model luminosities after a galaxy age corresponding to redshift z = 0.0044 (i.e. the redshift of the Virgo cluster) in the chosen cosmological model are scaled to the average observed B-band luminosity of the respective galaxy type in the Virgo cluster (cf. Sect. 5.2).

In the following we present as an overview the comparison of GALEV models for star clusters and for normal galaxy types E, Sa … Sd with observations and refer to previous papers for more details.

5.1 Star clusters

The colours from U through K predicted by GALEV models for SSPs or star clusters at an age of $\sim 12 - 13$ Gyr are in very good agreement with the respective observed colours for a large set of M31 and Milky Way globular clusters (Barmby et al. 2000; Barmby & Huchra 2000) at their

respective metallicities (cf. Schulz et al. 2002). Small deviations in the U- and B-bands can be explained by the existence of Blue Straggler stars (likely products of stellar mergers) in the dense cores of GCs, which can make significant contributions at those short wavelengths (Xin et al. 2007; Xin & Deng 2005; Cenarro et al. 2008), but are not included in our models yet, as standard isochrones exist for non-interacting single stars only. Further contaminants in the blue-to-UV region are Blue Horizontal Branch stars (Schiavon et al. 2004; Dotter et al. 2007) and to a lesser degree even Cataclysmic Variables and low-mass X-ray binaries in the far-UV range (Rich et al. 1993; Dieball et al. 2007).

As shown in Kurth et al. (1999) and Lilly & Fritze (2006), Lick indices for SSPs as calculated by GALEV agree well with Galactic and M31 globular cluster data as compiled by (Harris 1996) in his online catalog[1].

GALEV models for star clusters also show good agreement at an evolutionary age of $\sim 12 - 13$ Gyr with the empirical calibrations for colours $(B - V)$ and $(V - I)$ versus metallicity [Fe/H] for old Galactic and M31 globular clusters, as e.g. given by Couture et al. (1990) and Barmby et al. (2000) over the metallicity range $-2.3 \leqslant$ [Fe/H] $\leqslant -0.5$ of these clusters. They also show, however, significant deviations from a linear extrapolation of these empirical relations towards higher metallicities, and they also show that the empirical relations are only valid for the *old* globular clusters for which they have been derived. Models can, of course, be used to study the behaviour of colour – metallicity relations for any colour and as a function of time (cf. Schulz et al. 2002, for details).

In Figure 5 we plot the evolution of three SSP models with different metallicities ranging from the lowest available value of [Fe/H] $= -1.7$ to the solar value [Fe/H] $= 0.0$. For comparison we also show V-K colours from Persson et al. (1983) for star clusters in the Large Magellanic Cloud, colour-coded according to their metallicity as derived from CMDs Mackey & Gilmore (2003). Our models are able to not only reproduce the full range of observed colours, but also match the colour-evolution of each metallicity subpopulation if accounted for typical uncertainties of 0.4 dex in the age-determination. For the old and metal-poor globular clusters our predicted V-K colours are in good agreement with observations.

As shown in Lilly & Fritze (2006), GALEV models for SSPs also agree, after $12-13$ Gyr of evolution with empirical calibrations of Lick indices vs. [Fe/H]. However, they also show that *all metal-sensitive indices are also age-dependent* and that the famous *age-sensitive* H_β and H_γ *indices are also metal-dependent* to some extent (see also Thomas et al. 2003; Korn et al. 2005). Hence, the empirical calibrations of Mg_2, Mgb, etc. vs. [Fe/H] are valid only for *old* (i.e. > 10 Gyr) globular clusters.

Empirical calibrations for colours or Lick indices vs. metallicity or age should therefore not be used for star clusters or globular clusters for which it is not a priori clear that their properties fall within the range of the calibrating Galactic clusters. Instead a full set of colours and/or indices in comparison to an extended grid of models covering the
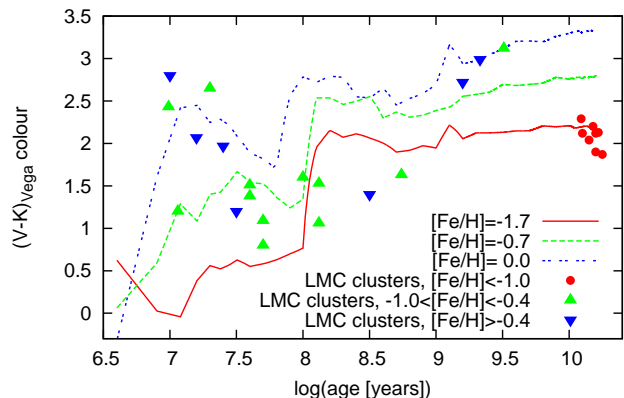

Figure 5. Evolution of the V-K colour of our SSP models with metallicities of [Fe/H] $= -1.7$ (red, solid line), [Fe/H] $= -0.7$ (green, dashed), and [Fe/H] $= 0.0$ (blue, dash-dotted). We also plot the data (ages from Mackey & Gilmore (2003), colours from Persson et al. (1983)) for 35 clusters in the Large Magellanic Cloud for comparison.
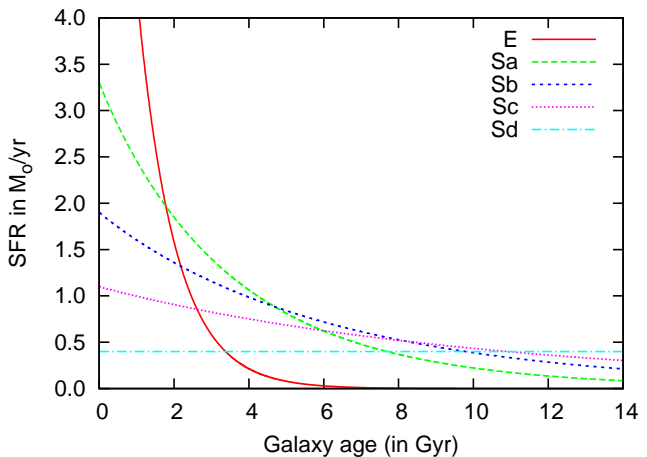

Figure 6. Star formation histories for the five different galaxy types E and Sa through Sd. Absolute numbers are normalized to a total galaxy mass of $10^{10} M_\odot$.

full parameter space, allows for independent and accurate determinations of both ages and metallicities (cf. Sect. 8.1).

5.2 Galaxies

By default, all our GALEV models for galaxies use a Salpeter IMF (Salpeter 1955) with lower and upper mass limits of $0.1 M_\odot$ and $100 M_\odot$, respectively.

The star formation histories, i.e. the time evolution of the star formation rates, of the different spectral galaxy types E and Sa to Sd are *the* basic parameters of GALEV and, in fact, of any kind of evolutionary synthesis models. In Fig. 6 we show SFHs for galaxies of different types from E through Sd, assuming the same total (i.e. stars and gas) mass M_{tot} of $10^{10} M_\odot$ for all of them. These SFHs are in good agreement with chemical and spectrophotometric findings from Sandage (1986).

For the elliptical model we use an exponentially declining SFR

---

[1] http://physwww.physics.mcmaster.ca/~harris/mwgc.dat

$$\Psi(t) = \frac{M_{tot}}{\alpha} \times \exp(-t/\tau) \tag{4}$$

with an e-folding time $\tau = 1\,$Gyr and $\alpha = 8.55 \times 10^8\,$yr.

For spectral types S0 and Sa through Sc the SFR is tied to the evolving gas content as given by

$$\Psi(t) = \beta \times \frac{M_{gas}(t)}{10^9}, \tag{5}$$

with efficiency parameters β decreasing from early to later spiral types, $\beta = 1.0\,$yr^{-1} for S0, $\beta = 0.33\,$yr^{-1} for Sa, $\beta = 0.19\,$yr^{-1} for Sb, and $\beta = 0.11\,$yr^{-1} for Sc galaxies.

Sd model galaxies are described by a constant SFR:

$$\Psi(t) = \psi_0 \times \frac{M_{tot}}{10^{10}} = const, \tag{6}$$

where $\Psi_0 = 0.4\,$M$_\odot\,$yr^{-1}.

For *closed-box models*, these parameters α, β, ψ_0, and τ are the only free parameters. We do *not* require additional parameters such as infall of gas or outflow in galactic winds to reproduce observations. Note that all these SFH parameters are independent of galaxy mass. We therefore do not reproduce mass-metallicity or colour-magnitude relations for galaxies of identical spectral types.

These SFHs are very similar in *all* evolutionary synthesis models (cf. e.g. Bruzual & Charlot 2003; Fioc & Rocca-Volmerange 1997). In detail, we adjust the SFH for the chemically consistent GALEV models as to match, after a Hubble time of evolution (i.e. $\approx 13\,$Gyr for our assumed concordance cosmology with H$_0 = 70\,$km s$^{-1}\,$Mpc^{-1}, $\Omega_M = 0.30$ and $\Omega_\Lambda = 0.70$), the observed

- average integrated colours from UV through NIR,
- average gas fractions,
- average metallicities,
- average present-day SFRs,
- average mass-to-light ratios, and
- template UV – optical spectra

of the respective spectral types as detailed below. All these observational constraints together very neatly define the average SFHs of undisturbed galaxies E, Sa, Sb, Sc, Sd and tightly constrain the few parameters describing them for a given IMF.

We stress that GALEV and all other evolutionary synthesis models with their respective SFHs are meant to describe *spectral types* of galaxies. And we caution that while in the Local Universe and for undisturbed galaxies a clear one-to-one correspondence is observed between spectral and morphological types, it is an open question how far back in time this correspondence might hold.

Gas fraction: The above described parameters have been tuned to reproduce the typical gas fractions observed in local galaxies (e.g. Read & Trentham 2005). We use gas contents, defined as fractions of gas relative to the total (gas+stars) mass, of $M_{gas}/M_{tot} = 0.0$ for E-models, 0.05 for Sa, 0.15 for Sb, 0.30 for Sc, and 0.55 for Sd models, respectively.

Colours: With these parameters being fixed, we compare a wide range of model-predicted colours from near-UV to near-IR to values from the literature. Our (B-V) colours, e.g. of 0.86 (E), 0.78 (Sa), 0.64 (Sb), 0.56 (Sc), and 0.43 (Sd) compare very well with the ranges found in the RC3
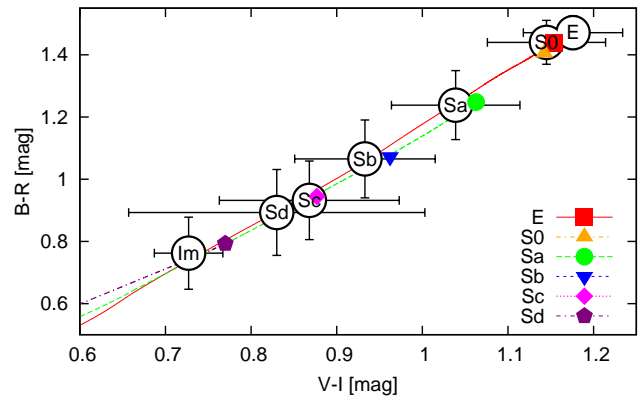

Figure 7. Evolution of galaxies of different types E through Sd in the (B-R)–(V-I) colour-colour-plane. Colours after 13 Gyr are plotted with large symbols. We also show colours for typical galaxies (large circles around galaxy type) taken from Buta et al. (1995) and Buta & Williams (1995).

catalog of de Vaucouleurs et al. (1995), listing mean colours of $(B - V) = 0.89^{+0.17}_{-0.53}$ (E), $0.74^{+0.25}_{-0.35}$ (Sa), $0.66^{+0.22}_{-0.47}$ (Sb), $0.51^{+0.22}_{-0.50}$ (Sc), and $0.44^{+0.22}_{-0.18}$ (Sd).

Spectra: In Fig. 5.2, we compare our model spectra to local templates for the galaxy types E, Sa, Sb, Sc, Sd from the catalog of Kennicutt (1992). As can be seen from those plots, the observed spectra for all spectral galaxy types from old passive ellipticals through the actively star forming Sd galaxies are well reproduced. Although our spectra (here using Lejeune's library) have a lower spectral resolution than the observed templates, they nonetheless reproduce all features, like absorption and emission lines. In the lower part of each plot we also show relative differences between model and template spectra. Deviations are generally smaller than differences between different galaxies of the same type, confirming the good agreement. Small differences for the emission lines originate in different spectral resolutions of templates and model spectra. Note that due to our chemically consistent treatment GALEV models can reproduce the Sd template spectrum with our Sd model at an age of 13 Gyr. This is a notable difference to all other evolutionary synthesis models that can only reproduce Sd template spectra with younger models of ages $4 - 6\,$Gyr (cf. Bruzual & Charlot 1993).

Metallicities: As mentioned above GALEV models calculate the time evolution not only of individual element abundances but also of the global ISM metallicity Z. After ~ 13 Gyr of evolution (for details on the evolution as function of age or redshift see Bicker et al. (2004) or Kotulla & Fritze (2009)), our models reach ISM abundances of $Z_E = Z_\odot$, $Z_{Sa} = 1.5\,Z_\odot$, $Z_{Sb} = 0.8\,Z_\odot$, $Z_{Sc} = 0.5\,Z_\odot$, and $Z_{Sd} = 0.25\,Z_\odot$. Those metallicities are in good agreement with typical ISM abundances, as measured at $1\,R_{eff}$, the effective or characteristic radius, of spiral galaxies of various types (Oey & Kennicutt 1993; Ferguson et al. 1998; van Zee et al. 1998). Note that our models aim to represent the *typical $L^\star$ or $M^\star$ galaxy of each spectral type*. Galaxies of different masses within the same spectral type are known to have slightly different metallicities, as described by the mass-metallicity or luminosity-
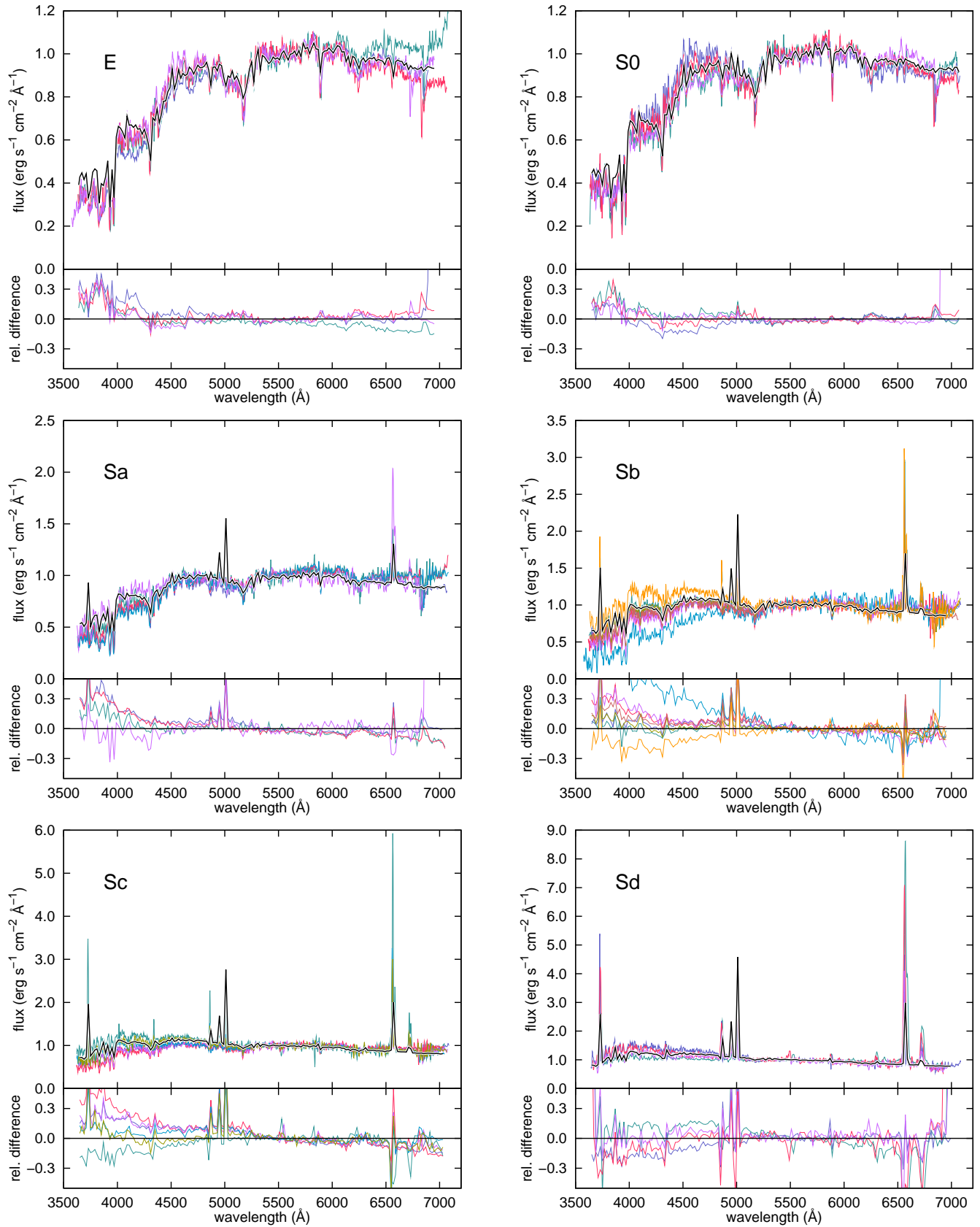
Figure 8. Comparison of model spectra of different types (top row: E and S0, middle row Sa and Sb, bottom row Sc and Sd) with observed template spectra from Kennicutt (1992). The black solid lines show the spectrum of GALEV models at an age of 12.8 Gyr, the coloured lines show spectra of several template galaxies of each respective type. In the lower part of each plot we also show relative differences between the GALEV spectra and each template spectrum.

metallicity relations (Skillman et al. 1989; Tremonti et al. 2004; Kewley & Ellison 2008). As stated before, these relations are currently not accounted for by GALEV standard models. However, the user is free to choose parametrizations of the SFHs as a function of galaxy mass (as, e.g., in Bressan et al. 1994) that reproduce these relations.

Star formation rates: GALEV models predict the following present-day SFRs Ψ_p in $[M_\odot \, \mathrm{yr}^{-1}]$ for the different spectral galaxy types: $\Psi_p \approx 0$ for E, $\Psi_p = 0.65$ for Sa, $\Psi_p = 0.4$ for Sb, $\Psi_p = 0.47$ for Sc, and $\Psi_p = 0.13$ for Sd galaxies. These numbers are in agreement with the average star formation rates of 0.22, 0.32 ± 0.2, 0.33 ± 0.14, and $0.09 \pm 0.03 \, M_\odot \, \mathrm{yr}^{-1}$ for Sa to Sd galaxies from Kennicutt (1983). We caution that the smooth SFHs in GALEV and other evolutionary synthesis models certainly are simplifications; real galaxies will in general experience fluctuations in their SFRs around these mean values. For the Milky Way, Rocha-Pinto et al. (2000) showed on the basis of individual stellar ages and abundances that the mean global SFH indeed fell nicely between those of our Sb and Sc models, with fluctuations of a factor of 2 on timescales of 100 Myr. Such fluctuations around the mean, however, do not significantly affect the long-term evolution.

Mass-to-light ratios: Using the stellar mass assembled after ~ 13 Gyr and the absolute V-band luminosity, we compute the V-band mass-to-light ratios. The results are: $M/L_V(E, Sa, Sb, Sc, Sd) = 11.8, 8.2, 5.9, 4.5, 3.0$, respectively. These include a factor that we call *fraction of visible mass* (FVM) and that accounts for the fraction of mass locked up in sub-stellar objects like brown dwarfs, planets, etc. This factor is set to FVM=0.5 in GALEV models, implying that only half the star formation rate forms luminous stars, while the remaining half is locked up in non-luminous objects (cf. Bahcall et al. 1992). Only with this FVM=0.5 can agreement with observed average M/L ratios (Faber & Gallagher 1979; Bell & de Jong 2001; Read & Trentham 2005) be achieved together with agreement in colours, spectra, and chemical abundances. Note that FVM does not include remnants of stellar evolution like white dwarfs, neutron stars or black holes; those are considered separately as part of stellar evolution.

Introducing the FVM parameter does not only affect the mass-to-light ratios but also has an impact on the chemical evolution with in turn impacts on most other derived parameters. A Salpeter IMF with mass-limits of 0.1 and 100 $M_\odot$ would lock up 60% of the mass in long-lived stars with $M \leqslant 1 \, M_\odot$, with the remaining 40% progressing the chemical enrichment of the galaxy. However, by applying a FVM=0.5 we half this fraction of stars with $M \geqslant 1 \, M_\odot$ so that now only 20% of stars return their ejecta at the end of their lifes, with the majority of mass being locked up. This concept to slow down the chemical enrichment is a common feature of many codes, but comes with different names, e.g. as free parameter $(1 - \xi)$ in Portinari et al. (1998).

Luminosity normalization With the SFHs as given above and a Salpeter IMF, GALEV models calculate the time evolution of spectra and luminosities in absolute terms as a function of the total mass, initially all in gas. Colours, of course, are independent of galaxy mass as GALEV models assume the SFH of each galaxy type to be independent of galaxy mass (see Fig. 6). Chemical ISM abundances are also

determined by this SFH *and* by the absolute level of SFRs in relation to the mass in the initial gas reservoir. Spectral fluxes and luminosities on the other hand are mass-dependent. If models of undisturbed galaxies are to be compared to observations of individual galaxies, it is important to calibrate their absolute luminosities to the observed ones, thereby also calibrating their (gaseous + stellar) masses and their SFRs.

Before we can compare models to distant galaxies, we need to calibrate their apparent magnitudes in the Johnson B-band against average observed magnitudes of the respective spectral galaxy types in the Local Universe. The average observed apparent luminosities of the different galaxy types in the Virgo cluster are given by Sandage et al. (1985a,b) to be $m_B(E) = 10.20$, $m_B(S0) = 12.60$, $m_B(Sa) = 11.95$, $m_B(Sb) = 12.90$, $m_B(Sc) = 12.83$, and $m_B(Sd) = 13.95$. The correction factors to match the computed and observed luminosities are then also applied to all mass-dependent model parameters, i.e. to stellar and gaseous masses, SFRs, etc.

5.3 Disturbed galaxies: Starbursts & SF truncation

In addition to the undisturbed galaxies above with their smooth and monotonically decreasing SFRs, GALEV can also describe the evolution of galaxies encountering fast changes in their SFR, e.g. a starburst with significantly enhanced star formation rate, or a truncation or strangulation of the star formation rate on some shorter or longer timescale, respectively. This allows us to study not only the spectral but also the chemical evolution of galaxies that experience starbursts or a quenching of their normal SFR, as they can occur e.g. during galaxy-galaxy interactions or mergers or in the course of the various transformation processes discussed for field galaxies that fall into galaxy clusters. We recall that GALEV models only deal with effects on the SFRs of galaxies and should be viewed as complementary to dynamical models describing the morphological transformations eventually related to these processes. Both starbursts and SF truncation/strangulation require additional free parameters. The first of these is the time of onset t_b, i.e. the age at which a previously undisturbed galaxy begins to feel changes in its SFR. Starbursts are described by a prompt increase in SFR followed by an exponential decline on some given timescale τ_b, that typically is of the order of a few hundred Myr for normal-size galaxies and of order $10^5 - 10^6$ yr for dwarf galaxies.

Across the literature, a number of different definitions for the strength of a burst are in use. The strength of a burst is either described by the amount of stars formed during the burst as compared to the stellar mass at the beginning or at the end of the burst or by the amount of all gas available at t_b that is transformed into stars during the burst, equivalent to the star formation efficiency (SFE) of the burst. We prefer the latter definition and define the burst strength via the star formation efficiency of the burst:

$$\mathrm{SFE(burst)} = \frac{\text{stellar mass formed during burst}}{\text{gas mass available at onset of burst}} \quad (7)$$

This definition limits burst strengths to be within the range $0 \ldots 1$ and gives, at the same time, a measure of the global SF efficiency during the burst. Please note that since

the burst strength depends on the amount of gas available at the onset of the burst, bursts of the same strength but occuring at different times and/or in galaxies of different types do not necessarily form the same amount of *stars*. E.g. a strong burst in an old and gas-poor Sa galaxy will form a much smaller mass of new stars than a weak burst early in the life of a gas-rich Sd galaxy. All burst strengths can only be determined at the end of the bursts. Before the end of the burst only lower limits can be estimated.

A truncation or strangulation of the SFR, e.g. as a galaxy falls into a galaxy cluster and has its HI stripped by ram pressure, is described either by an abrupt termination of SF or an exponential decline of the SFR on a timescale τ_b. After a burst or after SF truncation/strangulation, GALEV models can have SFRs going either exponentially to zero or to some constant low level.

6   THE WEB INTERFACE

We present the new web interface that enables everyone to run her or his model of choice in a fast, easy to learn and easy to use, and comfortable way over the internet. The interface can be found at

http://www.galev.org

Using a web interface enables us to impose some checks previous to program execution dealing with the most serious and frequently occuring problems. For the user this has the important advantage of always having the latest version at hand, including the most up-to-date input physics like isochrone sets and stellar libraries.

6.1   How to use the web-interface

The web-interface consists of four steps: Two for the input of the model parameters and the requested output, one for parameter checking and at last the actual running of the program on the web-server.

6.1.1   Principal model parameters

On the first page the user has to decide which type of model (s)he wants to run. Those defining parameters are

(i) **Galaxy type**: choose between the most common types E, S0, and Sa to Sd for undisturbed galaxies, for which the parameters described in Sect. 5.2 will be used. In addition we offer *free* types, defining the shape of the SFH as described by eqs. 4–6. We also offer instantaneous burst (SSP) models, as well as completely definable SFHs. For the latter mode the user has to specify a file with SFRs as function of time in the next step.

(ii) **Burst**: we currently offer three possibilities: *No burst*, i.e. an undisturbed galaxy, a *Burst* with given strength, duration, and exponentially declining SFR, beginning at some time t_b and *SF Truncation* with the SFR declining exponentially to zero on some specified timescale, again from time t_b on.

(iii) Number of filters for which magnitudes are to be computed.

If the user chooses to run a standard model for an undisturbed galaxy, i.e. an elliptical or spiral galaxy, then GALEV in the following uses the parameters described in Sect. 5.2. For all other cases, i.e. either user-defined galaxy types or models with burst/truncation, the parameters will be entered in the following step.

6.1.2   Model configuration

Depending on the choices from the previous page the user might not have all possible parameters to choose from; only the ones required for the specified model type will be shown. Those are:

(i) We offer a set of **Initial Mass Functions (IMF)**, namely from Salpeter (1955) and Kroupa (2001), both using the Lejeune (Lejeune et al. 1997, 1998) stellar atmosphere library. Further IMF shapes (e.g. Chabrier 2003) and different sets of stellar libraries are in preparation. In a future release we plan to also allow the user to choose customized IMFs; this feature, however, will be limited to SSP models (i.e. for star clusters).

(ii) **Gaseous emission** can be switched off or on, and the user can choose to include only continuum emission or both continuum and line emission. In fixed metallicity models, the gaseous emission is evaluated for the respective metallicity, in the chemically consistent case, it is calculated appropriately as described in Sect. 3.3.

(iii) The **metallicity**: choose between *chemically consistent* models, i.e. those including all enrichment effects described above, or a model with metallicity fixed to one of the following values $[\text{Fe/H}] = -1.7, -0.7, -0.4, 0.0, +0.4$.

(iv) The **galaxy type** is shown as a reminder, but cannot be changed here any more. To change the type the user has to go back to the first step.

(v) **Galaxy mass** is another free parameter, mainly used for normalization. We do not include a mass-metallicity relation of any kind, so this parameter has no impact on the resulting colours. Note that when GALEV is combined with a cosmological model to e.g. obtain apparent magnitudes, the model galaxy mass can optionally gets rescaled to match, after a Hubble time, the average B-band luminosity of local galaxies of the respective type in Virgo.

(vi) **SFH parameters**: if (and only if) one of the free models has been chosen, then the variables α (normalization for the SFR of an elliptical model), τ (e-folding timescale of an elliptical model), β (factor of proportion for spiral models), and ψ_0 (constant SFR of an Sd model) can be freely chosen by the user. The meaning of those parameters is explained in more detail in Sect. 5.2. If in the previous step the user requested the SFH to be read from a file this will be specified here. We caution the reader to carefully study the web-output from GALEV, since depending on the chosen parameters there might be problems, e.g. a SFR exceeding the amount of gas that is available.

(vii) If the user wants to compute a galaxy featuring a **burst** or SF **truncation**, then (and only then) he/she has to specify the time of the onset of the burst, expressed in years after galaxy formation and the e-folding timescale for the decline of the SFR during the burst. While those two parameters are common to both truncation and burst, only in the latter case one also needs to supply a burst strength.

Following our definition of the burst-strength in Sect. 5.3 (eq. 7), this specifies the fraction of gas available before the burst that is to be converted into stars during the burst. If one instead wants to specify the SFR at the very onset of the burst, $SFR(t = t_b)$, those two numbers can be converted into each other by $b = SFR(t = t_b) \times \tau_b / M_{gas}(t = t_b)$.

(viii) GALEV currently supports two different **extinction laws** that can be applied to the spectra, the Calzetti et al. (1994) law for starburst galaxies, and the Cardelli et al. (1989) Milky Way extinction law, using the standard value of $R_V = 3.1$. To compute colours for different extinction values, the user can specify a maximum E(B-V) value and a step-size. The output (see below) will then include multiple files, one for each extinction value in the requested range.

(ix) **Cosmological parameters** need to be specified to model the evolution of galaxies with redshift. The user can choose Hubble constant H_0, Ω_M, and Ω_Λ, while Ω_K is fixed to 0. To convert ages into redshifts the user also has to select a formation redshift z_{form}, so that the age of the galaxy is given by $age(z) = t_H(z) - t_H(z_{form})$ with t_H being the Hubble time at redshifts z and z_{form}. Note that the modeling process is terminated at a galaxy age of 16 Gyr. A choice of cosmological parameters leading to a galaxy age of more than 14 Gyr (e.g. too low a Hubble constant) hence results in an error-message, so that no colours will be computed for this case.

(x) Although GALEV offers a full range of different output options (see below), not all the numbers will be actually needed for any specific application. The user can therefore use the section **Output parameter** to restrict the output, leading to faster execution and smaller downloads.

(xi) To compute magnitudes from the spectra the user can choose from a large list of **filter functions** and also specify the magnitude system on which magnitudes are to be based (Vega, AB or ST magnitudes) For each filter a different magnitude system can be chosen. This eliminates the uncertainties involved in any *a posteriori* transformations between different systems.

We also offer an extensive online help giving examples for different parameters and how they affect the resulting SFH.

6.1.3 Output

In the following we will describe which outputs are available and also how they are computed.

(i) The **integrated spectra for each timestep** are the most important output, since from those all magnitudes and redshifted spectra are derived.

(ii) Convolving the spectra with the appropriate filter functions and applying the appropriate zeropoints gives us the **magnitudes** of the model as a function of time.

(iii) GALEV also delivers the most useful diagnostic data for each timestep, such as current **stellar and gaseous mass**, **star formation rates**, **ISM metallicity**, and ionizing flux N_{LyC}.

(iv) After applying a cosmological model to convert galaxy age into redshift (assuming a formation redshift) we can compute the redshifted galaxy spectrum, that includes all evolutionary effects. We also apply the intergalactic attenuation from Madau (1995) to account for absorption of flux shortwards of Lyα by intervening neutral hydrogen clouds.

(v) Convolving those redshifted spectra with filter functions FF(λ) and adding the bolometric distance modulus gives us apparent magnitudes with and/or without attenuation, that then can be used e.g. for comparison with observed SEDs to derive photometric redshifts or ages and metallicities.

(vi) From the data described above we can derive cosmological corrections due to the shifting of the filter functions to shorter restframe wavelengths (k-corrections) and evolutionary corrections (e-corrections). Those corrections are computed as follows:

$$k(z) = -2.5 \times \log \frac{\int_0^\infty f(t = t_0, z, \lambda) \times FF(\lambda) d\lambda}{\int_0^\infty f(t = t_0, 0, \lambda) \times FF(\lambda) d\lambda} \tag{8}$$

$$e(z) = -2.5 \times \log \frac{\int_0^\infty f(t = t(z), z, \lambda) \times FF(\lambda) d\lambda}{\int_0^\infty f(t = t_0, z, \lambda) \times FF(\lambda) d\lambda} \tag{9}$$

where $f(t, z, \lambda)$ is the flux at wavelength λ of a galaxy of age t at redshift z, t_0 the current age of the universe (which depends on the specified cosmological parameters), and FF(λ) a filter function.

6.1.4 Parameter checking and execution

As a third step in the modeling process we perform a quick check to ensure that all required parameters are given and correspond to valid combinations. The page also displays all given parameters to allow the user to check the input, and eventually perform corrections by going back to the previous page. However, the tests performed are just basic validity tests and do not ensure that the computed model makes physical sense.

In the fourth and last step, after the user has made sure that all input is correct, we create all files necessary for the actual modelling. The execution of the GALEV program takes several minutes to run. We urge all users to carefully read through the given output to check if everything ran smoothly.

Directly after GALEV has created all spectra, it computes the magnitude evolution as a function of time or redshift in all filters requested, again taking a few minutes to complete.

For compatibility reasons all output is given as human-readable ascii-files, with values aligned in columns that are separated by spaces, so that the files can be easily analysed and/or plotted. The resulting files are then automatically combined and compressed into one archive (.tar.gz) file, that can be downloaded. Each archive also contains a small ReadMe file listing the content of each file. The meaning of individual columns are specified at the beginning of each file.

6.2 Upcoming features of the web-interface

In its current version the web-interface supports the most frequently used GALEV features like computing spectra and colours. Further features, like the computation of Lick indices or colour magnitude diagrams are currently in the pro-

cess of being adapted and implemented into the webpage and will be accessible online in the near future.

7 FUTURE PROSPECTS

In the near future (Weilbacher et al. 2009, in prep.) we will offer further stellar libraries, e.g. Munari et al. (2005) and Coelho et al. (2005), to be able to compute high-resolution spectra for comparison with modern spectroscopic surveys. Those libraries have higher spectral resolution and shorter wavelength coverage but are not colour-corrected in the way Lejeune et al. (1997, 1998) did for the Kurucz spectra to reproduce the observed colours of stars from the UV through the NIR over the full range of effective temperatures.

One drawback of current galaxy evolutionary synthesis models is that they do not include a self-consistent treatment of dust absorption and reemission. One factor contributing to this difficulty are geometric effects and dependencies of dust masses and properties on gas content, chemical abundances and eventually even radiation field. Early attempts to consistently include dust absorption as a function of gas content and [Fe/H] in collaboration with D. Calzetti were encouraging (cf. Möller et al. 2001) and showed that every undisturbed galaxy goes through a phase of maximum extinction of $E(B - V) \sim 0.4$. The redshift of this maximum $E(B - V)$ phase is determined by the interplay between decreasing gas content and increasing metallicity. The predicted values at high-redshift $z \approx 3$ (equivalent to a galaxy age of ≈ 2 Gyr) agree well with observations from Steidel et al. (1999), Shapley et al. (2001) and Colbert et al. (2006).

Another aspect is the coupling of GALEV to a dynamical model (SPH + N-body + SF + feedback) to cope with increasingly available data from Integral Field Units allowing spatially resolved spectroscopy. Our early attempt to couple GALEV models for single stellar generations with a cosmological structure formation simulation by M. Steinmetz was encouraging (cf. Contardo et al. 1998) and showed that this approach is feasible. The simulated HST images of a galaxy at different redshifts showed fairly good agreement with observations but ultimately failed to reproduce the correct local disk sizes and parameters. A better and more detailed description of feedback seems to be required. This can only be obtained from an extensive comparison between model results and resolved galaxy observations. The key issue is to have a correct criterion for SF and a correct description of feedback on the relevant scales and over the full range of SF activity – from the lowest levels in the farthest outskirts of galaxies to the highly clumped and clustered SF in the strongest starbursts.

8 APPLICATIONS

GALEV models have a wide range of applications from star clusters and resolved stellar populations of nearby galaxies through integrated properties of galaxies up to the highest redshifts. A fair number of them have been explored so far, many of them hand in hand with refinements or special features added to the models. Here we briefly recall a few of them to illustrate the various features of GALEV.

8.1 Star clusters

The simplest stellar systems to study with GALEV are star clusters, so-called simple stellar populations (SSPs) where all stars are formed essentially within one timestep and with the same chemical abundances. GALEV models describe the time evolution of SSPs with different metallicities, including the gaseous emission during early evolutionary stages and as appropriate for their respective metallicity. They can also incorporate extinction within the clusters' parent galaxy on the basis of empirical extinction laws from Calzetti et al. (1994) or Cardelli et al. (1989).

Using our AnalySED tool (Anders et al. 2004b,a), we can compare observations in widely spaced broad-/mediumband filters to a grid of GALEV models and derive physical cluster parameters such as ages, masses, metallicity, and extinction between the cluster and the observer If one of the parameters can be externally constrained (e.g. dust-free environment, or metallicity previously determined from spectroscopy) observations in at least 3 bands are required, otherwise at least 4 bands are needed. As a large number of star clusters can usually be covered by a single set of observations, this is a very efficient way to study statistically significant cluster samples.

As shown both in studies based on artificial star clusters and on star clusters with ages and metallicities derived independently from CMDs, accuracies in age determination of Δage/age $\leqslant 0.3$ and in metallicity determinations of Δ[Fe/H]/[Fe/H] $\leqslant 0.2$ are achievable, preferably if both a short-wavelength band (U or B) and a NIR-band are included (Anders et al. 2004a; de Grijs et al. 2003a; de Grijs & Anders 2006). The U-band is crucial for accurate age-dating, and a NIR-band (H or K) for accurate abundances. We successfully applied these models in Anders et al. (2004b) to the interpretation of the young star cluster systems in the starburst dwarf galaxy NGC 1569, in Anders et al. (2007) to the analysis of the star clusters in the interacting Antennae galaxies (NGC 4038/39), and in Kotulla et al. (2008) to the derivation of ages and metallicities of the globular clusters in the Virgo S0 galaxy NGC 4570.

8.2 Colour-magnitude diagrams

One special feature of GALEV is its ability to compute colour-magnitude diagrams (CMDs) in any desired passband combination. This is possible not only for SSPs or instantaneous bursts, but also for composite stellar populations with complex SFHs. This has successfully been used to identify the best possible passband combination to disentangle age and metallicity effects in star clusters in various age ranges (cf. Fritze et al. 2006).

In Fritze & Lilly (2007) we compared the SFH obtained from the CMD with those obtained from the integrated spectrum, from Lick index measurements and from multi-band photometry in their respective accuracies and limitations. The basic result was that none of the methods allows to look back beyond a recent burst or some recent phase of enhanced SFR, and that all methods face very similar accuracy limitations at look-back times beyond ~ 1 Gyr. Only within the most recent Gyr, CMD analysis achieves the most detailed SFHs (cf. Lilly & Fritze 2005b,a). The importance of this

kind of comparative investigation lies in the fact that CMD analyses can only be done for the resolved stellar populations within the nearest Local Group galaxies. All attempts to explore the SFHs of more distant galaxies have to rely on integrated spectra and, for the most distant ones, on integrated photometry only.

8.3 Undisturbed galaxies

In Bicker & Fritze (2005) we used GALEV models to study the effects of the chemical evolutionary state of galaxies on their star formation rate indicators (Hα, [OII], NUV and FUV luminosities) and found that *all of them* significantly depend on metallicity, with errors in the worst cases of up to factors of a few, confirming previous observational evidence (e.g., Jansen et al. 2001; Hopkins et al. 2003; Kewley et al. 2004).

In Schulz et al. (2003) study the time and redshift evolution of bulge-to-disk light ratios in different wavelength bands by assuming a short timescale for SF for the bulge component $\Psi_{bulge} \sim \exp(-t/1\,\mathrm{Gyr})$ and a constant SFR for the disk component $\Psi_{disk} \sim$ constant. The integrated spectral and photometric evolution of different spiral galaxy types was then obtained by adding up the bulge and disk components in mass ratios so as to give, after a Hubble time of evolution, the observed average B-band bulge-to-disk light ratios for the respective spiral types Sa through Sd. This study showed a significant wavelength dependence of the bulge-to-disk light ratios in agreement with observations by Eskridge et al. (2002). This has implications for galaxy classification in different redshift intervals. It also opens a new possibility to explore bulge formation scenarios and bulge formation redshifts by comparing bulge-to-disk light ratios measured in different bands.

8.3.1 Starbursts in Blue Compact Dwarf Galaxies

Starbursts were first investigated with GALEV models in the context of Blue Compact Dwarf Galaxies (BCDGs) in a series of papers by H. Krüger (Krüger et al. 1991, 1992, 1993; Krüger & Fritze 1994; Krüger et al. 1995). These authors investigated a sample of BCDGs with optical and NIR photometry in order to derive their burst strengths and the age of their underlying stellar population. The main results we want to recall here are that even very weak ongoing bursts can completely dominate the light in the optical, in particular at the low metallicities $Z_\odot/50 \ldots Z_\odot/5$ typical for BCDGs. An underlying old galaxy component can only be detected in the NIR and was found for every BCDG of our sample. Very accurate age-dating was possible for those BCDGs which showed a 4600 Å bump caused by WR-stars in their spectra. Burst strengths were found to be of the order of a few percent only, when defined in terms of stellar mass increase. They were also shown to systematically decrease with increasing galaxy mass, where the latter included the important mass contributions of HI. This result is in agreement with expectations on the basis of the stochastic self-propagating SF scenario put forward by Gerola & Seiden (1978) and Seiden & Gerola (1979).

8.4 Interacting galaxies and mergers

In Fritze & Gerhard (1994a,b) we studied a grid of starburst models with bursts of various strengths occurring in Sa, ..., Sd spirals at different ages in their spectral, photometric and chemical evolution and then analyzed the starburst in the gas-rich massive spiral-spiral merger NGC 7252. We found this burst to have started about $600 - 900\,\mathrm{Myr}$ ago and to have been stronger by $1 - 2$ orders of magnitude than those in BCDGs. The bulk of information available for this galaxy even allowed us to estimate the SF efficiency on the basis of a comparison of the stellar mass formed during the burst.

Our conservative estimate for the overall SF efficiency (see equation 7) during this interaction-induced starburst indicated a very high value SFE $\geqslant 0.35$ (Fritze & Gerhard 1994a,b; Fritze & Burkert 1995), again about two orders of magnitude higher than any SFE measured for molecular clouds in the Milky Way or the Magellanic Clouds, and high enough to allow for the formation of a new generation of globular clusters (cf. Brown et al. 1995; Li et al. 2004). GALEV models indicated that NGC 7252 at present still features a low-level ongoing SFR of $\sim 3\,\mathrm{M_\odot\,yr^{-1}}$ in its centre, powered for $\sim 50\,\%$ by gas set free at present from dying burst stars and for $\sim 50\,\%$ by HI falling back onto the main body from the tidal tails. Both of these gas delivery rates will decrease over the next $1 - 3\,\mathrm{Gyr}$. Depending on whether the SFR will cease completely or continue at some very low level, NGC 7252 will spectrally evolve into an elliptical or S0 galaxy over the next $1 - 3\,\mathrm{Gyr}$. Already at present, NGC 7252 features an $r^{1/4}-$ light profile across a radial range of ~ 14 kpc, if azimuthally averaged (Schweizer 1982)

Independent confirmation for the unexpectedly high value found for the SFE in NGC 7252 came from the detection of a rich population of massive compact star clusters with ages in agreement with the global starburst age which, in turn, is in agreement with dynamical merger ages from N-body + SPH simulations (e.g. Hibbard & Mihos 1995). Spectroscopy of the brightest clusters confirmed their metallicities to be between $Z_\odot/2$ and $Z_\odot$, as expected if they formed out of the gas pre-enriched in Sc-type spirals – with some evidence for a moderate amount of self-enrichment during the burst on the basis of their slightly enhanced [α/Fe] ratios. In Fritze & Burkert (1995) we estimated that the number of clusters with masses in the range of Galactic globular cluster (GC) masses that formed in the burst and survived until the present is of the same order of magnitude as the number of GCs present in two average-luminosity Sc-type spirals before the merger. Hence, this spiral-spiral merger will, after the fading of the post-starburst and after the fading and dissolution of the tidal features, evolve into an elliptical or S0 galaxy with a normal GC specific frequency. GCs of age $0.5 \ldots 1$ Gyr have already survived the most critical phase in their lives, the infant mortality and early mass loss stages, and stand fair chances to survive for many more Gyr (cf. Lamers et al. 2005; Bastian & Goodwin 2006; Parmentier & Fritze 2009).

In de Grijs et al. (2003b) we used GALEV SSP models to analyze the luminosity-weighted ages pixel-by-pixel on ACS images of the interacting galaxies Tadpole and Mice and studied their star cluster populations. A surprising result was that about 35 % by mass of all recent SF went into the formation of star clusters in both galaxies, not only across

the main bodies of both galaxy systems but all along their very extended tidal tails.

In Temporin & Fritze (2006) we applied GALEV models to investigate the SF and starburst histories of galaxies in a very compact group of galaxies on the basis of multiband photometry and spectra and in Wehner et al. (2006) we studied the SF activity and its history in the extended tidal debris surrounding the starburst galaxy NGC 3310.

8.4.1 Tidal Dwarf Galaxies

Not only star clusters can form in the low-density environments of tidal tails but sometimes even star-forming objects with masses in the range of dwarf galaxies: so-called Tidal Dwarf Galaxies (TDGs), or better TDG candidates. In Weilbacher & Fritze (2001) and Weilbacher et al. (2002, 2003b,a) we analyzed the first reasonably sized sample of TDGs and found that they all contain a stellar population inherited from the spiral disk out of which the tidal tail has been torn, together with a significant young stellar population that must have been formed *in situ* within the tidal tail after it had been ejected. A characteristic feature of TDGs is that they do not follow the luminosity-metallicity relation of dwarf galaxies but all have similar metallicities characteristic of the HII region abundances in spiral disks.

Again it turned out that optical observations alone are not sufficient to disentangle the mass contributions of the inherited versus the starburst components. Even a 90 % mass fraction in the inherited component can be entirely hidden in the optical by an ongoing burst that only makes up for 10 % of the mass. Only in optical-NIR colours can the inherited component be detected that is not entirely old but contains the mix of stellar ages present in the disk before the tidal tail was thrown out.

8.5 Galaxy transformation in groups and clusters

A variety of scenarios are discussed in the literature to explain the transformation of the spiral-rich field galaxy population into the S0-/dSph-/dE-rich galaxy population observed in rich galaxy clusters at low redshift. The following processses have been proposed: High-speed disruptive galaxy-galaxy interactions called harassment, interactions between galaxies and the dense hot Intracluster Medium (ICM), and enhanced merging within infalling groups. All of these scenarios are observed to be at work in a number of individual cases. Their relative importance, their timescales, transition stages, and end products, however, are not known yet. All of these transformation processes both affect the morphological appearance of galaxies and – via their SF histories – their spectral properties. How the timescales for morphological transformation and spectral transformation relate to each other in the various scenarios and environments is not clear to date. Removal of gaseous halos, outer, and inner HI disks leads to SF strangulation on long timescales or to SF truncation on shorter ones. Destabilization of disks through encounters or shocks as well as mergers within infalling groups may lead to starbursts. We explored aspects related to the spectral transformation of galaxies through all these scenarios and investigated which scenarios in which type of progenitor galaxy and at which

evolutionary stage can lead to the observed luminosity and colour ranges of S0 galaxies by implementing SF strangulation/truncation on different timescales with and without preceding starbursts into GALEV models in Bicker et al. (2002). In Falkenberg et al. (2009a,b) we extended the models to also include the evolution of the D4000 and Hδ Lick indices into the GALEV models for galaxy transformation and investigated under which conditions the so-called E+A-, or k+a-, and the Hδ-strong galaxies (cf. Poggianti et al. 2004; Dressler et al. 2004) are formed, what is the lifetime of this respective phase, what is the colour and luminosity of the galaxy in this transition stage and what is the end-product.

8.6 High redshift galaxies and photometric redshifts

If coupled to a cosmological model, GALEV can be used to study the evolution of galaxies from the very onset of SF in the early universe until today. Accounting for the significantly sub-solar metallicities observed at high redshifts – in particular when dealing with intrinsically faint galaxies that dominate in deep field surveys – allows us to determine more accurate photometric redshifts, as compared to those obtained with solar-metallicity models only (Kotulla & Fritze 2009) or observed templates (Kotulla 2009, *in preparation*).

In Fritze & Bicker (2006) we examined starbursts and their respective post-starburst stages across a wide range of redshifts with the surprising result that dust-free models in their long post-burst phases after strong starbursts at high redshifts can get the colours and luminosities of Extremely Red Objects (EROs) as e.g. observed in the K20-survey (cf. Daddi et al. 2002; Cimatti et al. 2002).

Only when we also include – in addition to our set of undisturbed models E, Sa, ..., Sd – the very blue starburst phases and also their *extremely red postburst phases* can we reproduce the full range of colours observed e.g. in the Hubble Deep Fields (Kotulla & Fritze 2009, in preparation). In Fig. 9 we show the F606W-Ks (approx. V-K) colour evolution for a set of undisturbed models E, and Sa through Sd, and for models with major starbursts (burst strengths chosen to consume 70% of the in each case available gas) occurring at different ages in a previously undisturbed Sb galaxy. A comparison to the photometric galaxy catalog of Fernández-Soto et al. (1999) for the HDF shows that GALEV models can describe the full colour range, even without any dust. Note that dust certainly plays a role in ongoing starbursts but not any more during postburst stages. Apparently, as observed in the local Universe, galaxies use up and destroy part of their dust in starbursts, while the rest is blown away by the end of the burst.

8.7 Redshift evolution of ISM abundances: spiral models vs. DLAs

The SFHs of our closed-box model galaxies were constrained by requiring agreement after 12−13 Gyr of evolution not only with observed spectrophotometric properties of the various galaxy types but also with their gas content and ISM abundances (cf. Sect. 5.2). While this ensures agreement at the present stage it needs not necessarily imply agreement over the entire evolutionary path. Some subtle interplay between SFR and infall rate, e.g., could lead to the present-day
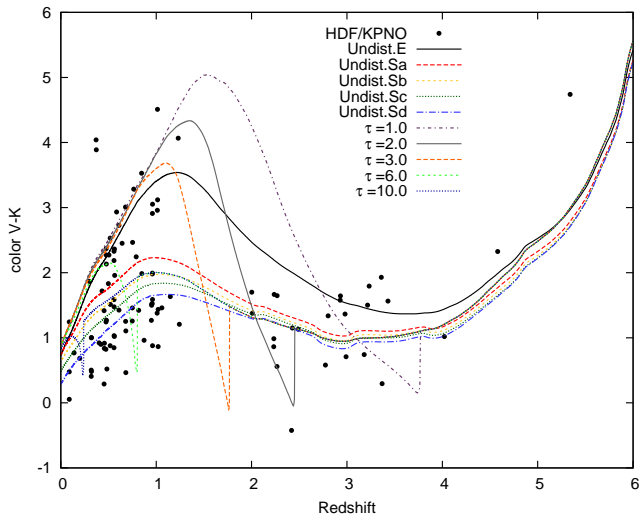
Figure 9. V-K colour as function of redshift for five undisturbed spectral types E and Sa through Sd. Extremely blue colours are found during active starbursts, while extremely red colours can be reached during the postburst phases of early starbursts, here shown for galaxy ages of 1, 2, 3, 5, and 10 Gyr.

agreement after ages of disagreement. Infall rates are very hard to constrain from a comparison with spectrophotometric properties alone. They can, however, be constrained by comparing chemical abundances. It is therefore of prime interest to compare the redshift evolution of ISM abundances to observations of high-redshift galaxies.

Transforming the time evolution of ISM abundances into a redshift evolution only requires the one-to-one transformation between galaxy age and redshift that is given by any set of cosmological parameters (see. Sect. 3.9)

Damped Lyman-α absorbers (DLAs) are a particular class of absorption systems, usually observed in the line-of-sight of quasars, with damping wings on the Lyman-α line due to the high column densities of neutral hydrogen of $N(HI) \geqslant 10^{21}$ cm^{-3} in the absorbers. The damped Lyman-α line is always accompanied by a number of low-ionisation heavy element lines, many of which are the dominant ionisation states in those absorbers. DLAs are most easily observed in the redshift range z $\sim$ 2 to z $>$ 4 and have been proposed to be potential progenitors of present-day spiral disks: Their HI column densities are similar to those in local gas-rich disks and their gas content, derived from rotational velocities of the order $100 \ldots 200 km\,s^{-1}$, is similar to gaseous plus stellar masses in local spirals. In Lindner et al. (1999) we compared the redshift evolution of our spiral galaxy models, calculated in a chemically consistent way with stellar yields for a large number of elements and 5 different stellar metallicities to the first reasonably sized set of Keck HIRES abundances for DLAs from the literature. We found surprisingly good agreement for all the different abundances over the entire observed redshift range with our closed-box models.

Studying the impact of various amounts of infall showed that it was not possible to accommodate more than a moderate amount of infall, increasing the total mass from redshift 2 until the present by not more than a factor $\sim$ 2, without losing agreement with either the spectral or the chem-

ical properties or both, no matter how we tuned the SFH. We hence concluded that from a chemical evolution point of view DLAs might well be the progenitors of present-day spiral galaxies of all types Sa . . . Sd and that those are reasonably well described by closed-box or moderate-infall models. This implies that DLAs have already almost all the mass of present-day spirals – albeit almost completely in the form of HI gas. GALEV models indicated low stellar masses and low luminosities for DLA galaxies, in agreement with the large number of non-detections/upper limits. Mass estimates from rotation velocities derived from detailed modeling of asymmetries detected in some DLA profiles confirmed our mass predictions (cf. Wolfe et al. 2005). GALEV models also predicted a change in the DLA galaxy population from high to low redshift and showed that the DLA phenomenon can be understood as a normal transition stage in the life of every spiral. During their enrichment process to higher metallicities they convert their gas reservoir into stars, therefore get increasingly gas-poor so that above a certain metallicity they drop out of DLA samples due to too low a gas content (cf. Lindner et al. 1999, for more information). This is in agreement with observations that show the lowest redshift DLA galaxies to be low-luminosity late-type or irregular galaxies.

9   SUMMARY

This paper presents the GALEV evolutionary synthesis models for star clusters, undisturbed galaxies and galaxies with starbursts or/and star formation truncation now available on the web at

http://www.galev.org

We describe the input physics currently used, that will continuously be updated.

For a number of different stellar IMFs, the spectral evolution of star clusters of metallicities in the range $-1.7 \leqslant [Fe/H] \leqslant +0.4$ can be calculated, and a large number of filter systems are available for the photometric evolution as well as the full set of Lick absorption indices.

GALEV features a unique combination of characteristics that allow for what we call a *chemically consistent modelling* of the chemical evolution of the ISM together with the spectral evolution of the stellar component.

This means that the initial abundances of every stellar generation are accounted for by using input physics (stellar evolutionary tracks, stellar model atmospheres, gaseous line and continuum emission, stellar lifetimes, yields and remnant masses) appropriate for the increasing initial abundances present at the formation time of successive stellar generations. This chemically consistent modeling accounts for the observed broad stellar metallicity distributions in local galaxies as well as for the increasing importance of subsolar abundances in local late-type and low luminosity galaxies and in high redshift galaxies.

Galaxy models can be calculated either in the chemically consistent way or for some fixed metallicity upon request. Models give spectra, emission line strengths and Lick absorption features, photometric quantities for a large number of filter systems, and chemical abundances, gaseous and stellar masses, star formation rates, etc. in their time evolution for normal galaxies, galaxies with starbursts or/and

star formation truncation as specified by the user or for user customized star formation histories.

If a cosmological model is selected, all quantities are also provided in their redshift evolution, fully accounting for evolutionary and cosmological corrections and including the attenuation by intergalactic neutral hydrogen.

We present the models, the input physics they use, their calibrations, the web interface and some examples of selected applications for illustration and we discuss current limitations and future prospects.

ACKNOWLEDGMENTS

APPENDIX A: WORKING IN PICTURES

In the following we will present the workings of GALEV in a more vivid way by guiding the reader through a series of steps. We give examples for the input physics GALEV uses and show how this is used throughout the process of modelling a galaxy.

A1   General steps

In the first step we present how one gets from isochrones, a stellar IMF, spectral library, and atomic physics to an integrated isochrone spectrum. For this example we choose to work with isochrones from the Padova group, a Salpeter-IMF from $0.1 M_\odot$ to $100 M_\odot$ and stellar spectra from the Lejeune library, all using solar metallicity.

Step 1: Choose set of isochrones

Fig. A1 shows solar-metallicity isochrones for three different ages of 4 Myr, 100 Myr and 1 Gyr as a colour-magnitude diagram. For very young ages the main sequence reaches up to high masses and hence very high luminosities ≈ -10 mag. For the later stages the red giant branch (RGB) at $(B - V) \approx 1 \dots 1.4$ is clearly visible and also the asymptotic giant branch (AGB). Note that stars on the AGB can reach extremely red colours of $(B - V) \approx 4$ mag and at the same time get very bright in the NIR ($M_K \sim -10$ mag) during the thermal pulsation (TP) phase.
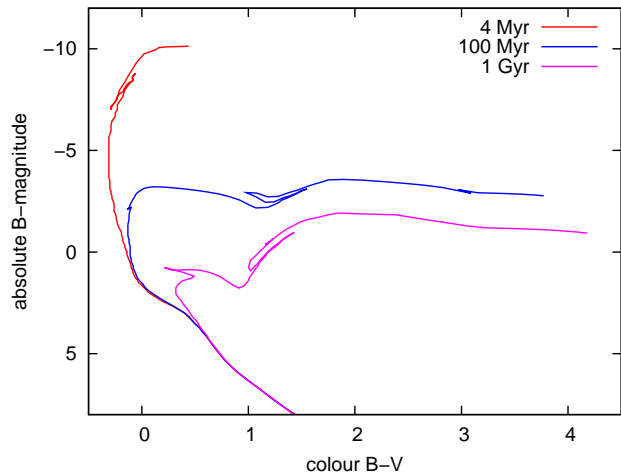
Figure A1. Solar metallicity isochrones from the Padova group for three different ages of 4 Myr, 100 Myr and 1 Gyr
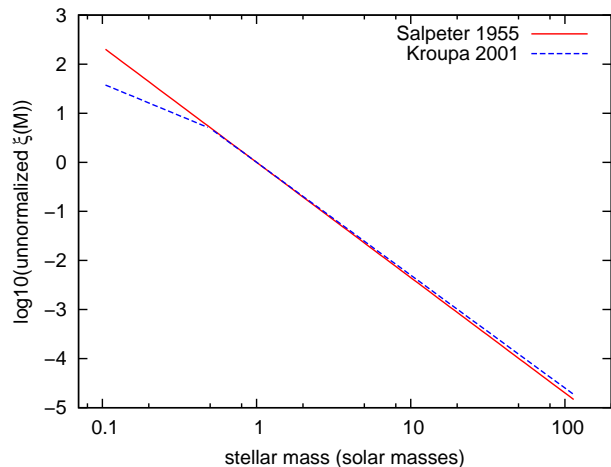

Figure A2. Two examples of initial mass functions, here from Kroupa (2001) and Salpeter (1955)

Step 2: Select Initial Mass Function

In a second step we have to choose a parameterization for the number of stars as function of their mass. Fig. A2 shows two common IMFs, the Salpeter and Kroupa IMFs. For masses $\geqslant 1 M_\odot$ both predict roughly comparable number of stars, but they differ in the low mass regime $\leqslant 1 M_\odot$. This will not only affect mass-to-light ratios, but also have an impact on the resulting spectra and in particular the chemical enrichment, since fewer low-mass stars also means that less mass gets locked up in long-lived stars.

Step 3: Populate isochrones with stars

With both isochrones and IMF at hand we can now populate the isochrones with stars taken from an IMF. For each mass point on the isochrone the IMF tells us how many stars were being formed with this mass. The results are shown in Fig. A3, where we also added some scatter around the individual points to give the artificial colour-magnitude diagram
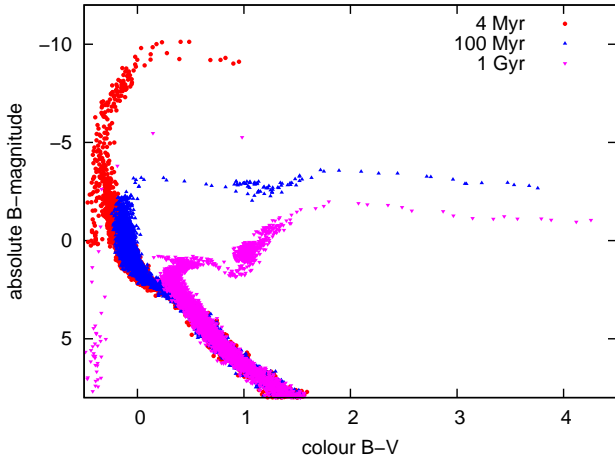
Figure A3. Synthetic colour magnitude diagram where each point from the isochrone is assigned a numbers of stars based on the IMF. We added some scatter around each point to produce a smoother appearance.

Figure A4. Sample spectra from the Lejeune stellar library for stars with $\log g = 4.0$ and $T_{\mathrm{eff}} = (20000, 10000, 5000, 2000)$K.

Figure A5. Integrated starlight for the three isochrones shown in Fig. A1.

a smoother and more realistic appearance. We also added at least one star to each point to bring out all phases of stellar evolution. However, in reality, this might not be the case, since some phases, e.g for very young and extremely hot white dwarfs last for a very short timescale only.

Step 4: Assign a spectrum to each star

Next we assign a spectrum to each star in the colour-magnitude diagram. The parameters required for this are either directly given in the isochrones (e.g. the effective temperature T_{eff}) or can be derived from other parameters (e.g. the surface gravity $\log g$ can be calculated from the stellar mass, its bolometric luminosity and effective temperature). In Fig. A4 we show four sample spectra for stars with identical $\log g = 4.0$, but temperatures ranging from $20000\,\mathrm{K}$ down to $2000\,\mathrm{K}$. Hot stars have a smooth slope and are bright in the UV. Stars with $T_{\mathrm{eff}} \approx 10000\,\mathrm{K}$ have prominent Balmer absorption lines characteristic for spectral type A stars. Cool stars are dominated by broad molecular absorption bands and only emit at long wavelengths. Not all stellar parameters are directly covered by the library, all other values have to be interpolated between neighbouring points in the library. Is is therefore crucial for the stellar library to cover the full parameter range.

Step 5: Integrate spectra of all stars

To create stellar isochrone spectra we now integrate the light of all stars. Special care has to be taken to account for the different luminosities of stars at their respective stages of evolution. In Fig. A5 we show spectra for the same ages discussed above, 4 Myr, 100 Myr, and 1 Gyr. The youngest spectrum is almost completely dominated by the hottest and brightest high-mass stars that also dominate part of the 100 Myr spectrum. For this spectrum the highest-mass stars have already exploded as supernovae and with them the flux in the FUV already has decreased considerably. In the optical the 4000Å break starts to appear, becoming stronger
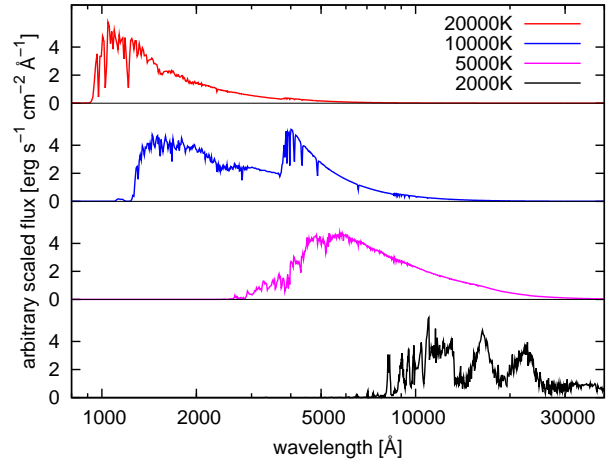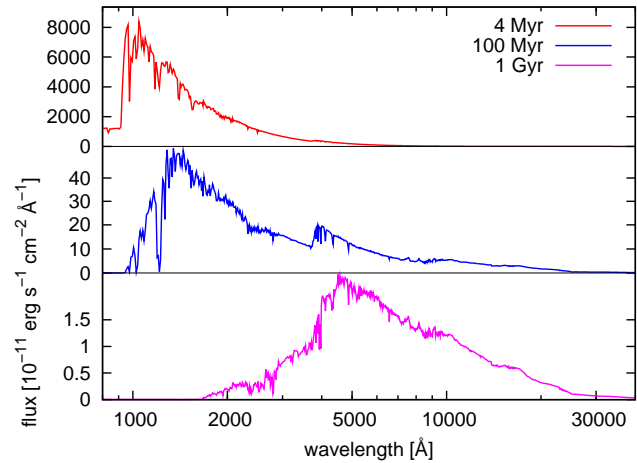
with time. After 1 Gyr there is little UV flux remaining, the spectrum is now dominated by stars with lower masses $\approx 2 M_\odot$.

Step 6: Compute gaseous line and continuum emission

Until now we have only dealt with stellar light. However, as mentioned earlier, at young ages isochrones contain large contributions from high mass stars. These emit a large fraction of their light in the UV and also produce significant numbers of photons energetic enough to ionize hydrogen. The energy injected into the surrounding interstellar medium produces both emission lines and also continuum emission. The detailed mechanisms of this are discussed in Sect. 3.3 and shown in Fig. A6. Note that while the strength of the heavy element emission lines depends on the metallicity of the gas, the strength of the continuum emission and hydrogen emission lines purely depends on the ionizing photon flux.
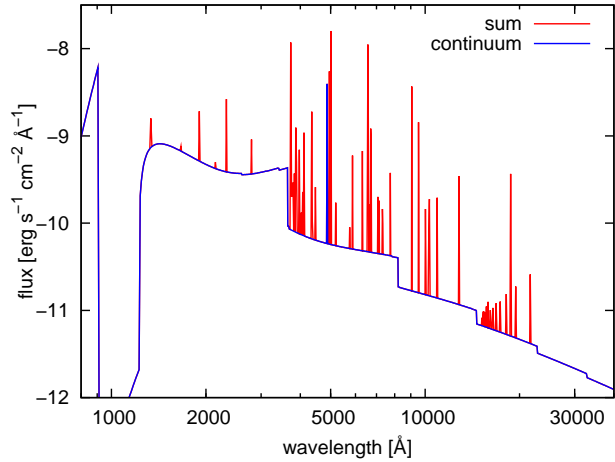
Figure A6. Gaseous emission spectrum for solar metallicity. Shown in blue is the continuum emission, and continuum and line emission in red.
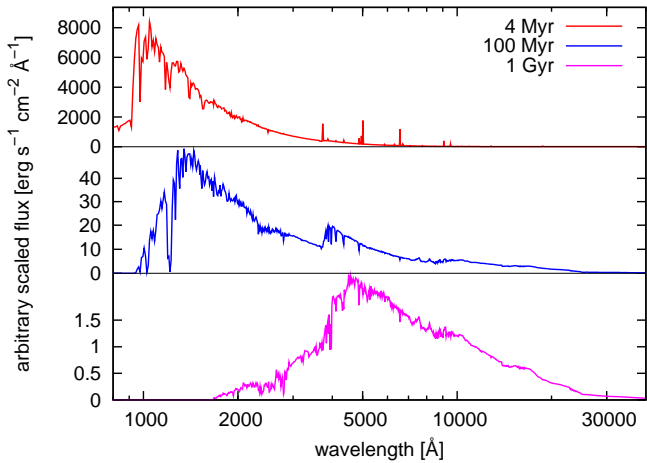

Figure A7. Integrated isochrone spectra for the same isochrones shown in Figs. A1 and A5, including both stellar and gaseous emission.

Step 7: Add gas emission to stellar spectrum

For each isochrone we now compute the gaseous emission spectrum based on the metallicity and ionizing photon flux derived from isochrones and IMF. Since the latter heavily depends on the age of the isochrone so does the strength of the gaseous emission. In Fig. A7 we show the same spectra as in Fig A5, but now with gaseous emission included. For the first spectrum at an age of 4 Myr the emission lines clearly stand out in the optical. However, for the later stages there are no changes compared to the purely stellar spectra, since only stars with masses $\gtrsim 20 M_\odot$ and hence very short lifetimes $\lesssim 10$ Myr produce the majority of the ionizing flux.

In GALEV those previous steps are repeated for all metallicities and ages available from the isochrone set, yielding a full set of isochrone spectra including both stellar and gaseous emission.
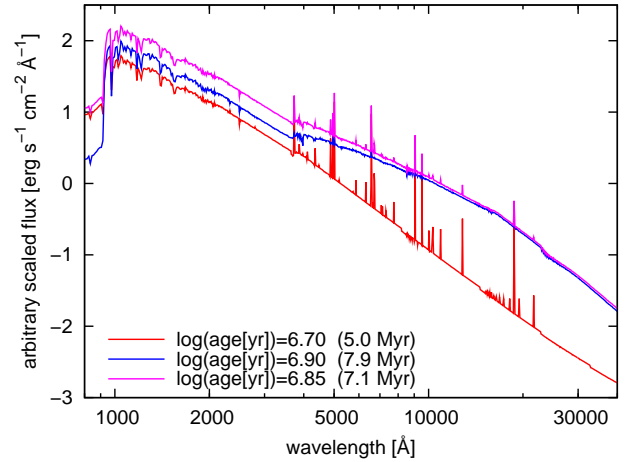

Figure A8. Example for contributing isochrone spectra during interpolation in age.

A2   Additional steps for star clusters

Continuing from the library of isochrone spectra GALEV can now compute the finer grid required for the study of star clusters.

Step 8: Interpolate between ages given by the isochrones

The time resolution offered by the isochrones in general only spans a relatively coarse grid with logarithmic age spacing. However, it is advantageous to create a grid with smaller and linear age steps. This can be done by interpolating additional ages to fill the gaps in the isochrone grid. Since spectra vary roughly linearly with logarithmic time, i.e. changes are larger at small ages and small at large ages we use this as basis for our algorithm. In Fig. A8 we show two isochrone spectra for ages of $\log(t) = 6.7$ and $\log(t) = 6.9$ and the resulting spectrum for $\log(t) = 6.85$. The resulting spectrum was computed by $\mathrm{Spec}(\log(t) = 6.85) = 0.25 \times (\mathrm{Spec}(\log(t) = 6.7) + 3 \times \mathrm{Spec}(\log(t) = 6.9)$.

To obtain a full grid to be used e.g. for age-dating star clusters one has to repeat this procedure for each required time step and each metallicity. The steps involved with applying dust extinction and computation of magnitudes from spectra is explained in Steps 11 and 14 below.

A3   Additional steps for galaxies

Galaxies are completely different from star clusters since they contain multiple stellar populations, generally covering a range of ages and metallicities. We explain the basic steps dealing with multiple populations based on a toy-model of a galaxy made from only two populations with different ages and metallicities. The subsequent explanations use the model of an undisturbed elliptical galaxy.

Step 8: Compute initial abundances for next generation

To derive the chemical evolution of galaxies we have to know four things: 1) The total mass of the galaxy, including both the mass of stars and gas. 2) The star formation history
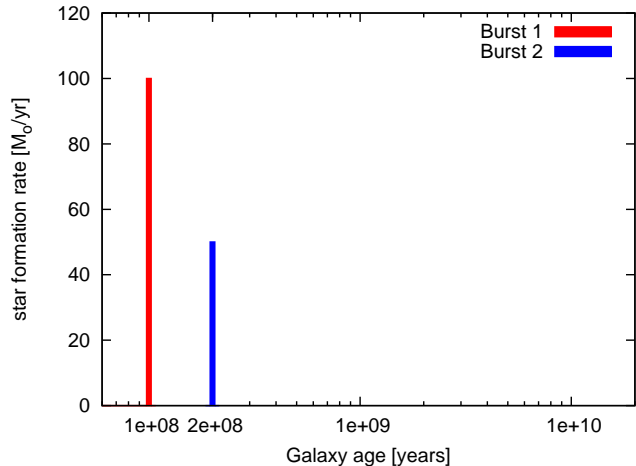
Figure A9. For our toy-model we construct a very primitive star formation history of 2 bursts, with SFRs of $100\,M_\odot\,yr^1$ and $50\,M_\odot\,yr^1$, each lasting 10^6 years.

(SFH), i.e. how many stars are formed at each particular time. 3) The life times of the stars formed. This in combination with the SFH yields some form of star death record. And we have to know 4) the end products of each star, i.e. the mass of its remnant, and the mass of gas and heavy elements returned to the surrounding ISM. For each time we then have to keep track of the masses of stars, gas and metals in the gas. All those quantities are changed by star formation and the return of gas and heavy elements from dying stars. The ratio of metals to gas is the crucial factor since it determines both the spectra and lifetimes of the newly formed stars.

Step 9: Interpolate between ages AND metallicities

For all galaxies with an extended SFH we will have stellar populations not agreeing with the coarse grid given by the isochrones. We therefore have to interpolate between isochrone spectra of different ages and also different metallicities. The details of this process are described in the context of star clusters above and are also shown in Fig. A8.

Step 10: Add up spectra weighted with SFH

To ease the understanding how GALEV assembles a galaxy spectrum from the individual spectra of each of its constituent populations, we first consider a toy model of a galaxy made from only two populations. Both populations are described by intervals of 1 Myr duration each, occuring at an age of 100 and 200 Myr and forming stars at a rate of $100\,M_\odot\,yr^{-1}$ and $50\,M_\odot\,yr^{-1}$, respectively (see Fig. A9). Both intervals are short compared to the age of the youngest isochrone so that they each can be described as a population of one age. We further assume that the earlier population (Burst 1) is formed with a metallicity of $[Fe/H] = -1.7$ or $1/50Z_\odot$, and the second (Burst 2) with a metallicity of $[Fe/H] = -0.7$ or $1/5Z_\odot$.

We will now show how to derive the spectrum of our toy-galaxy at two ages of 300 Myr and 1 Gyr. For each timestep
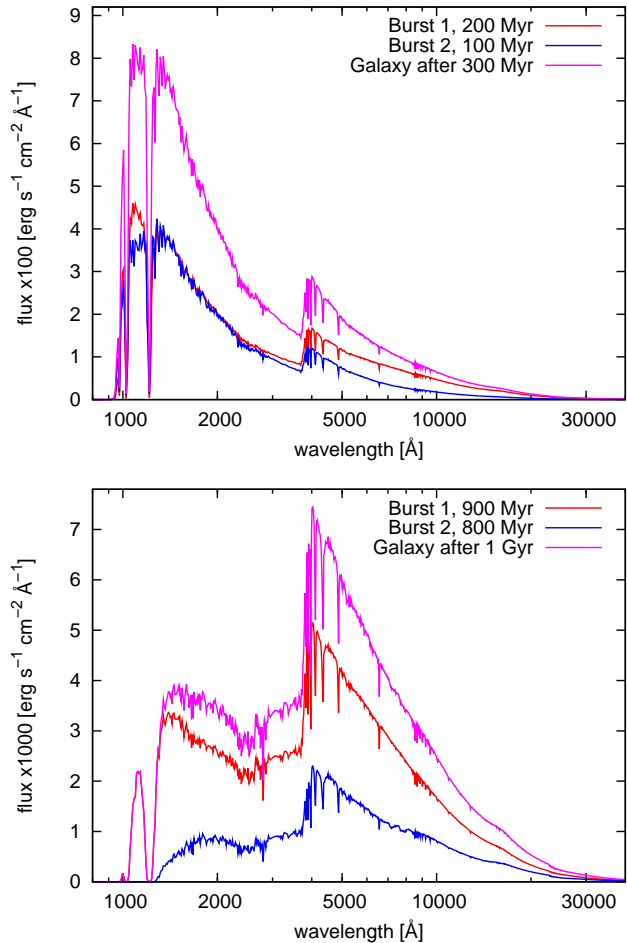

Figure A10. Interpolated isochrone spectra for each burst and the resulting galaxy spectrum, for galaxy ages of 300 Myr (top panel) and 1 Gyr (bottom panel).

t one needs to derive the ages τ and metallicities of all populations formed prior to this time. Those are then weighted by the SFR at their respective formation time $SFR(t - \tau)$ multiplied with the length of a time step. Those are then added up to yield the galaxy spectrum. For our toy galaxy at an age of 300 Myr we know that Burst 1 has metallicity $[Fe/H] = -1.7$ and an age of 200 Myr. Burst 2 has metallicity $[Fe/H] = -0.7$ and an age of 100 Myr. The resulting spectrum thus can be constructed by added up those two isochrone spectra. The resulting spectrum is shown in the upper panel of Fig. A10.

The spectra for all other times are created in a similar way. Metallicities for each population stay the same, while ages increase with time. The resulting spectrum of our toy-model galaxy at an age of 1 Gyr is shown in the bottom panel of Fig. A10

In the following we will leave our toy-model galaxy and instead show the remaining steps that are necessary to derive magnitudes for an elliptical galaxy with a small amount of dust at redshift z = 3.
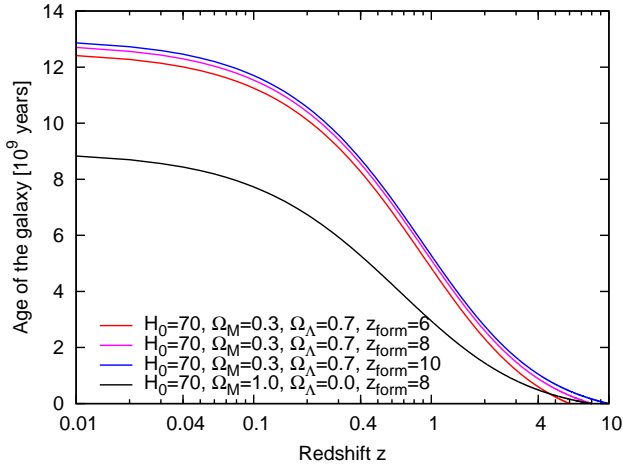
Figure A11. Relation between galaxy age and redshift for different cosmological parameters and in particular varying formation redshifts.

Figure A12. Extinction curves from Calzetti and Cardelli. Both show very little transmission at short wavelengths indicating that most of the light gets absorbed.

Step 11: Apply evolutionary correction

Since we want to model the galaxy at a cosmologically significant redshift of z = 3 we have to take evolutionary corrections into account, i.e. we observe the galaxy at an earlier evolutionary state. We therefore have to know the age of the galaxy at this redshift. In Fig. A11 we show the redshift-galaxy age relation for a small range of cosmological parameters. It is obvious that the density parameters Ω_M and Ω_Λ influence the solution, but also the formation redshift z_{form}, the redshift at which the galaxy started forming stars. The impact of those evolutionary corrections can be seen in Fig. A14. The first row shows the galaxy at redshift z=0 with an age of ≈ 13 Gyr. The second row shows the galaxy at its evolutionary state at z = 3; the galaxy at redshift 3 started forming stars only ≈ 1.5 Gyr earlier.

Step 12: Apply extinction

In a next step we apply the attenuation due to interstellar dust. For our example we choose the Calzetti et al. (1994) extinction law (see Fig. A12 and choose an intermediate degree of extinction, E(B-V)=0.2. For comparison we also show the dust attenuation curve of Cardelli et al. (1989). Both extinction curves have in common that the transmission, i.e. the fraction of light that remains unabsorbed, drops towards shorter wavelengths, leading to a reddening of the galaxy light. The results on the spectrum can be seen from the difference between the second and third row in Fig. A14

Step 13: Redshift spectrum

The spectrum now has to redshifted by a factor (1+z). Note that also the flux has to reduced by the same factor (1+z) to properly account for the cosmic expansion.

Step 14: Apply intergalactic attenuation curve

Due to the high redshift at which we observe our galaxy we have to correct for intergalactic absorption due to intervening neutral hydrogen clouds. These absorb light shortwards
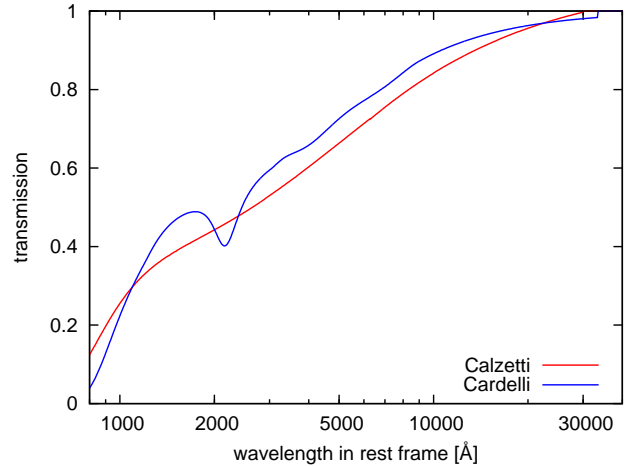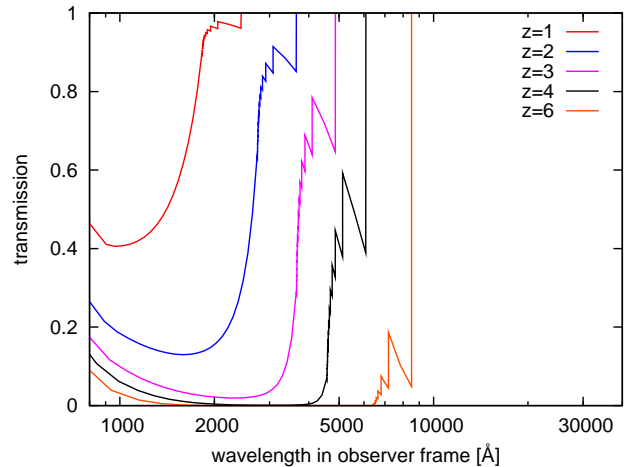

Figure A13. Transmission of the intergalactic medium as function of observed frame wavelength for sources at different redshifts.

of the Lyman-α line (1216 Å) and hence reduce the flux in this region. Fig. A13 shows the transmission of the IGM as function of observed frame wavelength for sources at different redshifts $z = 1 \ldots 6$. For a galaxy at redshift 3 this means that $\approx 30\%$ of the light between the Lyman-break (912 Å) and the Lyman-α line is absorbed, while shortwards of the Lyman-break essential all flux is absorbed (hence the name Lyman-break). Fig. A14 shows in the two bottom rows the spectrum with (5th row) and without (4th row) this attenuation.

All the previously mentioned effects are summarized in Fig. A14. The first row shows the spectrum of the galaxy at redshift $z = 0$ at an age of 13 Gyr. The second row still is at z = 0, but at an evolutionary state already corresponding to $z = 3$. The following panel shows the spectrum with a reddening of $E(B - V) = 0.2$ mag; Here most of the far-UV flux is already absorbed by dust. The fourth row shows the spectrum redshifted to z = 3 and the last row also takes intergalactic attenuation into account.
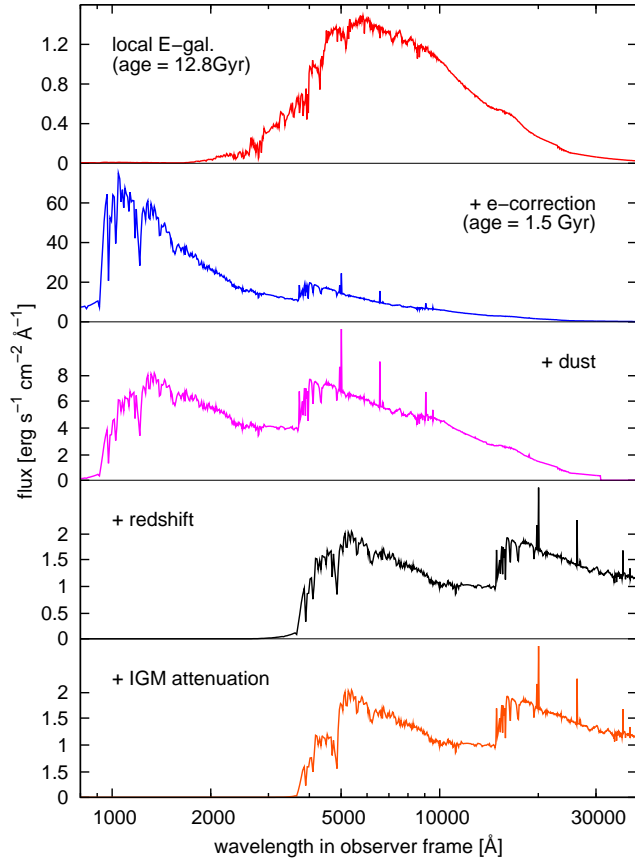
Figure A14. Galaxy spectrum of an elliptical galaxy at different stages of the modelling process. Each following spectrum includes all effects shown above.

Figure A15. Selection of the filters currently offered by GALEV, ranging from the far-UV to near-infrared.

Step 15: Convolve with filter response curve to compute magnitudes

We can now convolve the final spectrum with filter response curves. Therefore each point in the spectrum is weighted with the relative filter response at the corresponding wavelengths and then integrated over all wavelengths. To convert the resulting fluxes into observable magnitudes we have to apply zeropoints according to the requested magnitude system, e.g. Vega or AB. In Fig. A15 we show a wide selection of currently available filters from different space and ground-based telescopes.

Step 16: Add distance modulus

In a very last step we can convert the absolute magnitudes obtained with the filters into apparent magnitudes. This is done by simply adding the bolometric distance modulus for the particular redshift. In Fig. A16 we show the evolution of the distance modulus with redshift for a small selection of possible cosmological parameter sets. For the previously studied galaxy at redshift $z = 3$ we have to add a distance modulus of 47 mag.

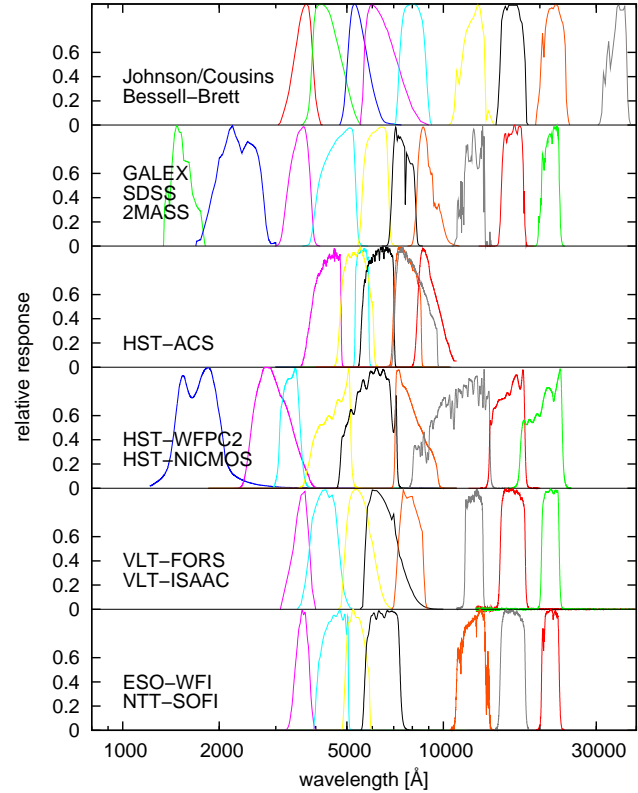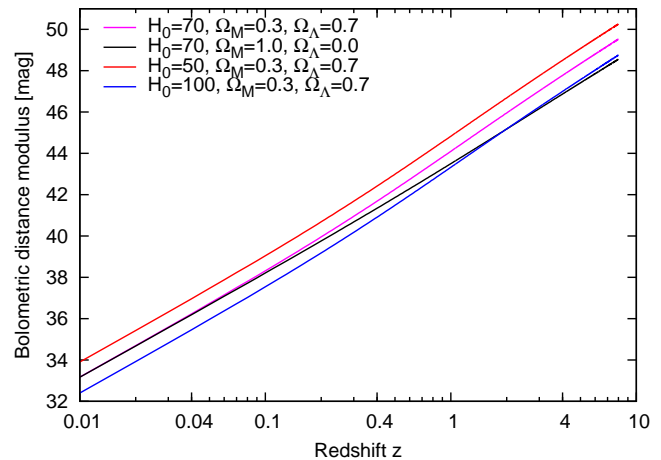This paper has been typeset from a TEX/ LATEX file prepared by the author.

Figure A16. Bolometric distance modulus as function of redshift for a range of cosmological parameter sets.

REFERENCES

Ak, S., Bilir, S., Karaali, S., Buser, R., & Cabrera-Lavers, A. 2007, New Astronomy, 12, 605
Allard, F., Hauschildt, P. H., & Schwenke, D. 2000, ApJ, 540, 1005
Aller, L. H., ed. 1984, Physics of thermal gaseous nebulae
Anders, P., Bissantz, N., Boysen, L., de Grijs, R., & Fritze, U. 2007, MNRAS, 377, 91
Anders, P., Bissantz, N., Fritze, U., & de Grijs, R. 2004a,

MNRAS, 347, 196

Anders, P., de Grijs, R., Fritze, U., & Bissantz, N. 2004b, MNRAS, 347, 17

Anders, P. & Fritze, U. 2003, A&A, 401, 1063

Bahcall, J. N., Flynn, C., & Gould, A. 1992, ApJ, 389, 234

Barmby, P. & Huchra, J. P. 2000, ApJ, 531, L29

Barmby, P., Huchra, J. P., Brodie, J. P., et al. 2000, AJ, 119, 727

Bastian, N. & Goodwin, S. P. 2006, MNRAS, 369, L9

Bell, E. F. & de Jong, R. S. 2001, ApJ, 550, 212

Bertelli, G., Bressan, A., Chiosi, C., Fagotto, F., & Nasi, E. 1994, A&AS, 106, 275

Bicker, J. & Fritze, U. 2005, A&A, 443, L19

Bicker, J., Fritze, U., & Fricke, K. J. 2002, A&A, 387, 412

Bicker, J., Fritze, U., Möller, C. S., & Fricke, K. J. 2004, A&A, 413, 37

Bohlin, R. C. & Gilliland, R. L. 2004, AJ, 128, 3053

Bressan, A., Chiosi, C., & Fagotto, F. 1994, ApJS, 94, 63

Bressan, A., Chiosi, C., & Tantalo, R. 1996, A&A, 311, 425

Brown, J. H., Burkert, A., & Truran, J. W. 1995, ApJ, 440, 666

Brown, R. L. & Mathews, W. G. 1970, ApJ, 160, 939

Bruzual, A. G. & Charlot, S. 1993, ApJ, 405, 538

Bruzual, G. & Charlot, S. 2003, MNRAS, 344, 1000

Bruzual A., G. 1983, ApJ, 273, 105

Buta, R., Corwin, Jr., H. G., de Vaucouleurs, G., de Vaucouleurs, A., & Longo, G. 1995, AJ, 109, 517

Buta, R. & Williams, K. L. 1995, AJ, 109, 543

Calzetti, D., Armus, L., Bohlin, R. C., et al. 2000, ApJ, 533, 682

Calzetti, D., Kinney, A. L., & Storchi-Bergmann, T. 1994, ApJ, 429, 582

Cardelli, J. A., Clayton, G. C., & Mathis, J. S. 1989, ApJ, 345, 245

Castellanos, M., Díaz, Á. I., & Tenorio-Tagle, G. 2002, ApJ, 565, L79

Cenarro, A. J., Cervantes, J. L., Beasley, M. A., Marín-Franch, A., & Vazdekis, A. 2008, ApJ, 689, L29

Chabrier, G. 2003, PASP, 115, 763

Cimatti, A., Mignoli, M., Daddi, E., et al. 2002, A&A, 392, 395

Coelho, P., Barbuy, B., Meléndez, J., Schiavon, R. P., & Castilho, B. V. 2005, A&A, 443, 735

Colbert, J. W., Malkan, M. A., & Rich, R. M. 2006, ApJ, 648, 250

Contardo, G., Steinmetz, M., & Fritze, U. 1998, ApJ, 507, 497

Couture, J., Harris, W. E., & Allwright, J. W. B. 1990, ApJS, 73, 671

Cunow, B. 2001, MNRAS, 323, 130

Cunow, B. 2004, MNRAS, 353, 477

Daddi, E., Cimatti, A., Broadhurst, T., et al. 2002, A&A, 384, L1

de Grijs, R. & Anders, P. 2006, MNRAS, 366, 295

de Grijs, R., Fritze, U., Anders, P., et al. 2003a, MNRAS, 342, 259

de Grijs, R., Lee, J. T., Mora Herrera, M. C., Fritze, U., & Anders, P. 2003b, New Astronomy, 8, 155

de Vaucouleurs, G., de Vaucouleurs, A., Corwin, H. G., et al. 1995, VizieR Online Data Catalog, 7155, 0

Dieball, A., Knigge, C., Zurek, D. R., et al. 2007, ApJ, 670, 379

Dopita, M. A., Groves, B. A., Fischera, J., et al. 2005, ApJ, 619, 755

Dotter, A., Chaboyer, B., Jevremović, D., et al. 2007, AJ, 134, 376

Dressler, A., Oemler, A. J., Poggianti, B. M., et al. 2004, ApJ, 617, 867

Ercolano, B., Barlow, M. J., Storey, P. J., & Liu, X.-W. 2003, MNRAS, 340, 1136

Ercolano, B. & Storey, P. J. 2006, MNRAS, 372, 1875

Eskridge, P. B., Frogel, J. A., Pogge, R. W., et al. 2002, ApJS, 143, 73

Faber, S. M. & Gallagher, J. S. 1979, ARA&A, 17, 135

Falkenberg, M. A., Kotulla, R., & Fritze, U. 2009a, ArXiv:0901.1665

Falkenberg, M. A., Kotulla, R., & Fritze, U. 2009b, submitted to MNRAS

Ferguson, A. M. N., Gallagher, J. S., & Wyse, R. F. G. 1998, AJ, 116, 673

Ferguson, A. M. N., Wyse, R. F. G., Gallagher, III, J. S., & Hunter, D. A. 1996, AJ, 111, 2265

Ferland, G. J., Korista, K. T., Verner, D. A., et al. 1998, PASP, 110, 761

Fernández-Soto, A., Lanzetta, K. M., & Chen, H.-W. 2003, MNRAS, 342, 1215

Fernández-Soto, A., Lanzetta, K. M., & Yahil, A. 1999, ApJ, 513, 34

Fioc, M. & Rocca-Volmerange, B. 1997, A&A, 326, 950

Fritze, U. & Bicker, J. 2006, A&A, 454, 67

Fritze, U. & Burkert, A. 1995, A&A, 300, 58

Fritze, U. & Gerhard, O. E. 1994a, A&A, 285, 751

Fritze, U. & Gerhard, O. E. 1994b, A&A, 285, 775

Fritze, U., Krüger, H., Fricke, K. J., & Loose, H.-H. 1989, A&A, 224, L1

Fritze, U. & Lilly, T. 2007, in Astronomical Society of the Pacific Conference Series, Vol. 374, From Stars to Galaxies: Building the Pieces to Build Up the Universe, ed. A. Vallenari, R. Tantalo, L. Portinari, & A. Moretti, 341–+

Fritze, U., Papaderos, P., Anders, P., et al. 2006, in IAU Symposium, Vol. 232, The Scientific Requirements for Extremely Large Telescopes, ed. P. Whitelock, M. Dennefeld, & B. Leibundgut, 241–247

Garcia Vargas, M. L. & Diaz, A. I. 1994, ApJS, 91, 553

Gauba, G., Parthasarathy, M., Nakada, Y., & Fujii, T. 2001, A&A, 373, 572

Gerola, H. & Seiden, P. E. 1978, ApJ, 223, 129

Girardi, L., Bressan, A., Bertelli, G., & Chiosi, C. 2000, A&AS, 141, 371

Gorgas, J., Faber, S. M., Burstein, D., et al. 1993, ApJS, 86, 153

Guiderdoni, B. & Rocca-Volmerange, B. 1987, A&A, 186, 1

Harris, G. L. H. & Harris, W. E. 2000, AJ, 120, 2423

Harris, G. L. H., Harris, W. E., & Poole, G. B. 1999, AJ, 117, 855

Harris, W. E. 1996, AJ, 112, 1487

Hibbard, J. E. & Mihos, J. C. 1995, AJ, 110, 140

Hopkins, A. M., Miller, C. J., Nichol, R. C., et al. 2003, ApJ, 599, 971

Hummer, D. G. 1988, ApJ, 327, 477

Inoue, A. K., Iwata, I., Deharveng, J.-M., Buat, V., & Burgarella, D. 2005, A&A, 435, 471

Izotov, Y. I. & Thuan, T. X. 1998, ApJ, 500, 188

Izotov, Y. I., Thuan, T. X., & Lipovetsky, V. A. 1994, ApJ, 435, 647

Izotov, Y. I., Thuan, T. X., & Lipovetsky, V. A. 1997, ApJS, 108, 1

Jansen, R. A., Franx, M., & Fabricant, D. 2001, ApJ, 551, 825

Kalirai, J. S., Hansen, B. M. S., Kelson, D. D., et al. 2008, ApJ, 676, 594

Kennicutt, Jr., R. C. 1983, ApJ, 272, 54

Kennicutt, Jr., R. C. 1992, ApJS, 79, 255

Kewley, L. J. & Ellison, S. L. 2008, ApJ, 681, 1183

Kewley, L. J., Geller, M. J., & Jansen, R. A. 2004, AJ, 127, 2002

Korn, A. J., Maraston, C., & Thomas, D. 2005, A&A, 438, 685

Kotulla, R. & Fritze, U. 2009, MNRAS, 393, L55

Kotulla, R., Fritze, U., & Anders, P. 2008, MNRAS, 387, 1149

Kroupa, P. 2001, MNRAS, 322, 231

Krüger, H. & Fritze, U. 1994, A&A, 284, 793

Krüger, H., Fritze, U., Fricke, K. J., & Loose, H.-H. 1992, A&A, 259, L73

Krüger, H., Fritze, U., Fricke, K. J., & Loose, H.-H. 1993, Ap&SS, 205, 57

Krüger, H., Fritze, U., & Loose, H.-H. 1995, A&A, 303, 41

Krüger, H., Fritze, U., Loose, H.-H., & Fricke, K. J. 1991, A&A, 242, 343

Kurth, O. M., Fritze, U., & Fricke, K. J. 1999, A&AS, 138, 19

Kurucz, R. L. 1992, in IAU Symposium, Vol. 149, The Stellar Populations of Galaxies, ed. B. Barbuy & A. Renzini, 225-+

Kučinskas, A., Hauschildt, P. H., Brott, I., et al. 2006, A&A, 452, 1021

Lamers, H. J. G. L. M., Gieles, M., & Portegies Zwart, S. F. 2005, A&A, 429, 173

Leitherer, C., Schaerer, D., Goldader, J. D., et al. 1999, ApJS, 123, 3

Lejeune, T., Cuisinier, F., & Buser, R. 1997, A&AS, 125, 229

Lejeune, T., Cuisinier, F., & Buser, R. 1998, A&AS, 130, 65

Li, Y., Mac Low, M.-M., & Klessen, R. S. 2004, ApJ, 614, L29

Lilly, T. & Fritze, U. 2005a, astro-ph/0507305

Lilly, T. & Fritze, U. 2005b, astro-ph/0507303

Lilly, T. & Fritze, U. 2006, A&A, 457, 467

Lilly, T. & Fritze, U. 2008, submitted to A&A

Lindner, U., Fritze, U., & Fricke, K. J. 1999, A&A, 341, 709

Mackey, A. D. & Gilmore, G. F. 2003, MNRAS, 338, 85

Madau, P. 1995, ApJ, 441, 18

Marigo, P., Girardi, L., Bressan, A., et al. 2008, A&A, 482, 883

Matteucci, F. & Padovani, P. 1993, ApJ, 419, 485

Matteucci, F. & Tornambe, A. 1987, A&A, 185, 51

Mezger, P. O. 1978, A&A, 70, 565

Möllenhoff, C., Popescu, C. C., & Tuffs, R. J. 2006, A&A, 456, 941

Möller, C. S., Fritze, U., Fricke, K. J., & Calzetti, D. 2001, Ap&SS, 276, 799

Munari, U., Sordo, R., Castelli, F., & Zwitter, T. 2005, A&A, 442, 1127

Nomoto, K. & Hashimoto, M. 1988, Phys. Reports, 163, 13

Nomoto, K., Iwamoto, K., Nakasato, N., et al. 1997, Nuclear Physics A, 621, 467

Nussbaumer, H. & Schmutz, W. 1984, A&A, 138, 495

O'Connell, R. W. 1976, ApJ, 206, 370

O'Connell, R. W. 1980, ApJ, 236, 430

Oey, M. S. & Kennicutt, Jr., R. C. 1993, ApJ, 411, 137

Oke, J. B. 1974, ApJS, 27, 21

Osterbrock, D. E. & Ferland, G. J. 2006, Astrophysics of gaseous nebulae and active galactic nuclei, 2nd. ed (University Science Books, Sausalito, CA)

Parmentier, G. & Fritze, U. 2009, ApJ, 690, 1112

Persson, S. E., Aaronson, M., Cohen, J. G., Frogel, J. A., & Matthews, K. 1983, ApJ, 266, 105

Pickles, A. J. 1985a, ApJS, 59, 33

Pickles, A. J. 1985b, ApJ, 296, 340

Pickles, A. J. & Visvanathan, N. 1985, ApJ, 294, 134

Piovan, L., Tantalo, R., & Chiosi, C. 2006a, MNRAS, 366, 923

Piovan, L., Tantalo, R., & Chiosi, C. 2006b, MNRAS, 370, 1454

Pipino, A. & Matteucci, F. 2004, MNRAS, 347, 968

Poggianti, B. M., Bridges, T. J., Komiyama, Y., et al. 2004, ApJ, 601, 197

Popescu, C. C., Misiriotis, A., Kylafis, N. D., Tuffs, R. J., & Fischera, J. 2000, A&A, 362, 138

Portinari, L., Chiosi, C., & Bressan, A. 1998, A&A, 334, 505

Prantzos, N., Vangioni-Flam, E., & Chauveau, S. 1994, A&A, 285, 132

Ramírez, S. V., Stephens, A. W., Frogel, J. A., & DePoy, D. L. 2000, AJ, 120, 833

Rauch, T. 2003, A&A, 403, 709

Read, J. I. & Trentham, N. 2005, Royal Society of London Philosophical Transactions Series A, 363, 2693

Rich, R. M., Minniti, D., & Liebert, J. 1993, ApJ, 406, 489

Rocha-Pinto, H. J. & Maciel, W. J. 1998, A&A, 339, 791

Rocha-Pinto, H. J., Scalo, J., Maciel, W. J., & Flynn, C. 2000, A&A, 358, 869

Sadler, E. M., Rich, R. M., & Terndrup, D. M. 1996, AJ, 112, 171

Salpeter, E. E. 1955, ApJ, 121, 161

Sandage, A. 1986, A&A, 161, 89

Sandage, A., Binggeli, B., & Tammann, G. A. 1985a, AJ, 90, 1759

Sandage, A., Binggeli, B., & Tammann, G. A. 1985b, AJ, 90, 395

Schaerer, D. & de Koter, A. 1997, A&A, 322, 598

Schiavon, R. P., Rose, J. A., Courteau, S., & MacArthur, L. A. 2004, ApJ, 608, L33

Schulz, J., Fritze, U., & Fricke, K. J. 2003, A&A, 398, 89

Schulz, J., Fritze, U., Möller, C. S., & Fricke, K. J. 2002, A&A, 392, 1

Schweizer, F. 1982, ApJ, 252, 455

Seiden, P. E. & Gerola, H. 1979, ApJ, 233, 56

Shapley, A. E., Steidel, C. C., Adelberger, K. L., et al. 2001, ApJ, 562, 95

Siana, B., Teplitz, H. I., Colbert, J., et al. 2007, ApJ, 668, 62

Silva, L., Granato, G. L., Bressan, A., & Danese, L. 1998, ApJ, 509, 103

Skillman, E. D., Kennicutt, R. C., & Hodge, P. W. 1989, ApJ, 347, 875

Smith, L. J., Norris, R. P. F., & Crowther, P. A. 2002, MNRAS, 337, 1309

Stasińska, G. 1984, A&AS, 55, 15

Steidel, C. C., Adelberger, K. L., Giavalisco, M., Dickinson, M., & Pettini, M. 1999, ApJ, 519, 1

Temporin, S. & Fritze, U. 2006, A&A, 447, 843

Thomas, D., Maraston, C., & Bender, R. 2003, MNRAS, 339, 897

Tinsley, B. M. 1968, ApJ, 151, 547

Tinsley, B. M. 1972, ApJ, 178, 319

Tinsley, B. M. H. 1967, PhD thesis, AA(THE UNIVERSITY OF TEXAS AT AUSTIN.)

Trager, S. C., Worthey, G., Faber, S. M., Burstein, D., & Gonzalez, J. J. 1998, ApJS, 116, 1

Tremonti, C. A., Heckman, T. M., Kauffmann, G., et al. 2004, ApJ, 613, 898

Truran, J. W. & Cameron, A. G. W. 1971, Ap&SS, 14, 179

van den Hoek, L. B. & Groenewegen, M. A. T. 1997, A&AS, 123, 305

van Zee, L., Salzer, J. J., Haynes, M. P., O'Donoghue, A. A., & Balonek, T. J. 1998, AJ, 116, 2805

Wehner, E. H., Gallagher, J. S., Papaderos, P., Fritze, U., & Westfall, K. B. 2006, MNRAS, 371, 1047

Weidemann, V. 2000, A&A, 363, 647

Weilbacher, P. M., Duc, P.-A., & Fritze, U. 2003a, A&A, 397, 545

Weilbacher, P. M. & Fritze, U. 2001, A&A, 373, L9

Weilbacher, P. M., Fritze, U., & Duc, P.-A. 2003b, Ap&SS, 284, 639

Weilbacher, P. M., Fritze, U., Duc, P.-A., & Fricke, K. J. 2002, ApJ, 579, L79

Weiss, A., Peletier, R. F., & Matteucci, F. 1995, A&A, 296, 73

Wise, J. H. & Cen, R. 2008, ArXiv:0808.2477

Wolfe, A. M., Gawiser, E., & Prochaska, J. X. 2005, ARA&A, 43, 861

Woosley, S. E. & Weaver, T. A. 1995, ApJS, 101, 181

Worthey, G., Faber, S. M., Gonzalez, J. J., & Burstein, D. 1994, ApJS, 94, 687

Worthey, G. & Ottaviani, D. L. 1997, ApJS, 111, 377

Xin, Y. & Deng, L. 2005, ApJ, 619, 824

Xin, Y., Deng, L., & Han, Z. W. 2007, ApJ, 660, 319